DISSERTATION

Umfassende Charakterisierung von zirkulierenden Tumorzellen für die Biomarkerentwicklung aus der Flüssigbiopsie

Comprehensive profiling of circulating tumour cells for development of liquid biopsy biomarkers

zur Erlangung des akademischen Grades
Doctor rerum medicinalium (Dr. rer. medic.)

vorgelegt der Medizinischen Fakultät
Charité – Universitätsmedizin Berlin

von

Stephanie Staudte

Erstbetreuung: Prof. Dr. Ingeborg Tinhofer-Keilholz

Datum der Promotion: 28.02.2025

:

Table of contents

List of tables

List of figures

List of abbreviations

BC	breast cancer
CPS	combined positivity score
CR	complete remission
CRC	colorectal cancer
CS	CellSearch® System
CTC	circulating tumour cell
EDTA	ethylenediaminetetraacetic acid
EGF	epidermal growth factor
EGFR	epidermal growth factor receptor
EMT	epithelial–mesenchymal transition
EpCAM	epithelial cell adhesion molecule
FCS /FBS	fetal calf serum / fetal bovine serum
FDA	food and drug Administration
γH2AX	phosphorylated form of the histone 2a variant
Gy	gray (unit of absorbed dose of ionizing radiation)
HNSCC	head and neck squamous cell carcinoma
ICI	immune checkpoint inhibitor
ISX	Amnis® ImageStream ® X Mk II Imaging Flow Cytometer
NSCLC	non-small cell lung carcinoma
OS	overall survival
PCR	polymerase chain reaction
PBMC	peripheral blood mononuclear cells
PBS	phosphate buffered saline
PD	progressed disease
PD–1	programmed cell death receptor 1

PD–L1	programmed cell death ligand 1
PD–L2	programmed cell death ligand 2
PFS	progression–free survival
PR	partial remission
RT	room temperature
SD	stable disease
TPS	tumour proportion score

Abstract

Solid tumours constantly shed tumour cells into the blood circulation and cells detach actively and intravasate into the blood system by undergoing an epithelial-to-mesenchymal transition (EMT). These so–called circulating tumour cells (CTCs) have been shown to be key players in metastasis, the main reason for cancer–related death. Detection of CTCs in peripheral blood has been established as prognostic biomarker for poor clinical outcome in various solid cancer types. However, although two CTC detection systems achieved clinical approval, methods for CTC quantification vary widely and no standard protocol has been established yet. Most of the currently used protocols rely on the detection of the epithelial cell adhesion molecule (EpCAM), which is expressed on epithelial CTCs, but downregulated in CTCs undergoing EMT. Consequently, the entire CTC population is not captured.

In my doctoral project, I aimed at establishing a novel CTC assay for comprehensive profiling of CTCs in order to exploit the entire potential of CTCs as a liquid biomarker to predict therapy response. The AMNIS® ImageStream®X MkII (ISX) imaging flow cytometer combines the power of high–throughput flow cytometry and high–resolution microscopy and thereby enables rapid and multiparametric phenotyping of CTCs. The protocol includes two tumour markers, the pan leukocyte marker CD45 and markers exploited as therapeutic targets, such as immune checkpoint molecules (PD–L1 /–L2), activation of cancer–associated pathways (phosphorylated EGFR) or response marker for radiotherapy (γH2AX foci). By using spiking experiments and a cut–off value of ≥ 3 CTCs /7.5ml blood, I could demonstrate a sensitivity of 73% at a specificity of 100%. A pilot study was performed to evaluate the applicability of the ISX protocol for CTC detection in patient blood samples [head and neck squamous cell carcinoma (HNSCC) n=16; breast cancer (BC), n=8]. Subsequently, a larger clinical study was conducted to determine the predictive and prognostic value of CTCs in recurrent /metastatic HNSCC patients (n=54), mostly treated with immune checkpoint inhibitors (ICI). Analysis revealed no prognostic value of CTC positivity, or a concordance of PD–L1 expression between tissue and liquid biopsy. Dynamic changes of CTC counts during treatment might be a better biomarker, enabling rapid real–time assessment of treatment responses. However, evaluation in a larger and more homogenously treated patient cohort is needed before conclusion can be drawn.

Zusammenfassung

Solide Tumore geben ständig Tumorzellen in den Blutkreislauf ab, welche sich aktiv ablösen und in die Blutzirkulation einwandern, indem sie eine epitheliale–mesenchymale Transition (EMT) durchlaufen. Diese sogenannten zirkulierenden Tumorzellen (CTCs) spielen nachweislich eine Schlüsselrolle bei der Metastasierung, dem Hauptgrund für krebsbedingte Todesfälle. Die Quantifizierung von CTCs wurde als negativer prognostischer Biomarker bei verschiedenen soliden Krebsarten entwickelt. Obwohl zwei CTC–Detektionssysteme klinisch zugelassen sind, gibt es noch keine Standardmethode für die CTC–Quantifizierung. Die meisten dieser Protokolle beruhen auf dem Nachweis des epithelialen Zelladhäsionsmoleküls (EpCAM), das auf epithelialen CTCs exprimiert wird, aber in CTCs unter EMT herunterreguliert ist. Folglich wird nicht die gesamte CTC–Population erfasst.

Ziel meines Projekts war die Etablierung eines neuen CTC–Tests zur umfassenden Charakterisierung von CTCs, um das gesamte Potenzial von CTCs als flüssiger Biomarker zur Vorhersage des Therapieansprechens auszuschöpfen. Das bildgebende AMNIS® ImageStream®X MkII (ISX) Durchflusszytometer kombiniert die Möglichkeiten der Hochdurchsatz–Durchflusszytometrie und der hochauflösenden Mikroskopie und ermöglicht so eine schnelle und multiparametrische Phänotypisierung von CTCs. Das Protokoll umfasst Marker zum Nachweis von Tumor–assoziierten Antigenen (EpCAM, EGFR), dem pan–Leukozytenmarker CD45, sowieso zur Analyse therapeutischer Targets, wie Immun–Checkpoint–Moleküle (PD–L1 /–L2), Aktivierungsstatus krebsassoziierter Signalwege (phosphorylierter EGFR) oder Ansprechmarker für Radiotherapie (γH2AX foci). Mit Hilfe von Spiking–Experimenten wurde eine Sensitivität von 73% und eine Spezifität von 100% bei einem Schwellenwert von ≥ 3 CTCs /7,5 ml Blut nachgewiesen.

In einer Pilotstudie wurde die Anwendbarkeit des ISX–Protokolls für den Nachweis von CTCs in Blutproben von Patienten [Plattenepithelkarzinom des Kopfes und Halses (HNSCC) n=16; Brustkrebs, n=8)] gezeigt. Anschließend wurde eine klinische Studie durchgeführt, um den prädiktiven und prognostischen Wert von CTCs bei rezidivierten /metastasierten HNSCC–Patienten (n=54) zu ermitteln, die überwiegend mit Immun–Checkpoint–Inhibitoren (ICI) behandelt wurden. Die Analyse ergab weder einen prognostischen Wert der CTC–Positivität noch eine Übereinstimmung der PD–L1 Expression zwischen Gewebe– und Flüssigbiopsie. Dynamische Veränderungen der

CTC–Zahlen während der Behandlung könnten ein besserer Biomarker sein, um eine schnelle Echtzeitbewertung des Ansprechens auf die Behandlung zu ermöglichen. Bevor jedoch Schlussfolgerungen gezogen werden können, ist eine Auswertung in einer größeren und homogeneren Patientenkohorte erforderlich.

1 Introduction

Cancer is one of the leading causes of death worldwide, accounting for one out of six deaths. Especially patients with metastasized stage of disease have a poor prognosis and treatment is challenging [Cancer (who.int), 10.11.2022]. Immense improvements have been achieved in cancer treatment in the last decade. Especially with the implementation of immune checkpoint inhibitors (ICI), the clinical outcome was improved in several malignancies, such as melanoma [1], head and neck squamous cell carcinomas (HNSCC) [2] or non–small cell lung carcinoma (NSCLC) [3].

Cancer diagnosis is generally based on clinical imaging, followed by either surgery and /or radiotherapy, chemotherapy, targeted therapy or ICI. These treatments can be administered either in combination or individually. Therapy selection is based on the analysis of the gene expression pattern of certain tumour biomarkers in the tumour tissue. Additional analysis for genetic alterations associated with therapy response or resistance is considered to reach a therapy decision.

Although tissue biopsy is still the gold standard, it has its limitations. Surgical removal of the tumour or collection of a tissue biopsy is sometimes not feasible due to the patient´s health condition, the localization of the malignant lesion or the risk of heavy side effects by the intervention itself. Additionally, it has to be considered that the conventional tissue biopsy does not reflect the entire intra–tumoural heterogeneity, resulting in an underestimation of tumours characteristics. Thus, there is still a significant number of patients not responding to biomarker–based selected treatment, frequently due to co–occurring mutations associated with resistance not detected by a single tissue biopsy. Conversely, there are patients who could have a clinical benefit from a specific treatment, but were not selected because they tested negative for a the corresponding biomarker [4].

Liquid biopsies represent a promising tool to circumvent the limitation of tissue biopsy in terms of capturing tumour heterogeneity between different spatial areas of a single tumour as well as between primary and metastatic lesions. Further, they are minimal–invasive, thereby allowing serial sampling for monitoring disease progression and treatment response. The term “Liquid biopsy” comprises all body fluids accessible for collection, such as saliva, urine, spinal and lymph fluids or blood. Circulating tumour DNA (ctDNA), extracellular vesicles and circulating tumour cells (CTCs) belong to the blood–

based liquid biomarkers and are under investigation to be used for treatment selection and response evaluation [5].

1.1 Circulating tumour cells

Metastasis and recurrence are the main reasons for cancer–related death. Strong efforts have been made to understand and reveal the multi–step cascade of metastasis [6], which might provide promising targets for new anti–cancer drugs. However, the entire process has not yet been deciphered. Tumour cells can intravasate into blood circulation or the lymphatic system either passively or actively. These so–called circulating tumour cells are either released by the tumour or detach actively from the bulk by undergoing epithelial–to–mesenchymal transition (EMT) [6]. Additionally, there is evidence that tumour cells undergo partial–EMT (pEMT), thereby gaining features of both epithelia and mesenchymal state. The pEMT state enables the maintenance of cell–cell interaction as well as the migration through the basement membrane to intravasate into the blood circulation, respectively [6]. Although a high amount of tumour cells is shed into the blood circulation every day, only a small subset survives shear stress, immune response or anoikis [6]. CTCs with a pEMT–like phenotype were shown to be resistant to anoikis and have a higher metastatic potential. CTCs can occur as single cells or as homogeneous and heterogeneous clusters composed of tumour cells or tumour and immune cells, respectively. Clusters were shown to have a higher metastatic potential compared to single CTCs [7]. CTCs display possibly different properties (tumour mutation burden, protein expression) of both the primary /recurrent tumour and the metastatic lesion, thereby enabling the analysis of the entire intra–tumoural heterogeneity [8]. Serial sampling of liquid biopsies allows for CTC–based monitoring of therapy response. Accordingly, promising personalized treatment decisions can be made, which may result in improved clinical outcome. Additionally, the detectable CTC count is demonstrated to be a prognostic factor in various solid cancer types, with ≥ 5 CTCs /7.5 ml in breast [9] or ≥ 3 CTCs /7.5ml in colon cancer [10], associated with worse prognosis.

1.2 CTC enrichment methods and detection

Isolation of CTCs is either based on their physical or immunological properties. Physical enrichment strategies rely on attributes such as size or deformability and do not require

any specific tumour marker. Immunological assays utilize a specific selection marker for CTC enrichment, subdivided in positive and negative enrichment. For positive enrichment, CTCs are detected through tumour–associated markers and isolated directly, while for a negative enrichment, leukocytes are labelled with CD45 and removed. The active removal of leukocytes results in a marker–independent CTC enrichment [11]. Subsequently, microscopy or imaging flow cytometry as well as molecular biological approaches (PCR) are used for CTC analysis. The U.S. Food and Drug Administration (FDA) approved two CTC detection devices for clinical use. While the most prominent device, the CellSearch® system (Veridex LLC; CS), was approved for BC in 2004 [9], the Parsortix® PC1 system (ANGLE PLC, UK) obtained FDA clearance in 2022.

To isolate CTCs using the CS, the blood samples are stained with anti–EpCAM antibodies coupled to magnetic particles, thus allowing a magnetic separation of CTCs from blood cells. The CTC–enriched cell suspension is further stained with anti–pan–cytokeratin as an additional epithelial marker and anti–CD45 to detect contaminating leukocytes. The CS is equipped with four detection channels and thus, only one channel is available for the analysis of an additional CTC–marker of interest. The Parsortix® is a microfluidic device using a cassette to perform a size–dependent CTC enrichment without the requirement of a tumor–specific marker. It was shown that CTCs are frequently larger than blood cells [11]. For subsequent CTC analysis, captured CTCs can be either stained “in–cassette” or harvested from it. However, multiparametric phenotyping of the captured CTCs using the Parsortix® requires an additional fluorescence microscope. Thus, both devices demonstrate limitations in terms of multiparametric phenotyping of CTCs.

Therefore, an imaging flow cytometer, such as the AMNIS® ImageStream® X Mk II (Cytek® Biosciences, CA, USA; ISX), might be a promising alternative for both devices. It combines the powerful tools of high–throughput flow cytometry and high–resolution microscopy. It can be equipped with up to six lasers and enables the simultaneous analysis of up to 12 markers. Moreover, two CCD cameras are integrated and an “extended depth field“ (EDF) module increases the field of depth of the image, increasing precision of intra–nuclear marker analysis.

1.3 Aim of the project

There is evidence that EpCAM alone is an insufficient tumour–marker for CTC detection, especially with respect to EMT–related heterogeneity of the CTC population. Therefore,

EpCAM–based CTC quantification does not cover the entire CTC population. Moreover, to be able to use CTCs not only for counting but also as a therapy–selection biomarker, a simultaneous expression analysis of potential therapeutic targets is indispensable. With respect to the aforementioned limitations of the two FDA–approved CTC detection devices, this project aimed at evaluating the suitability of the ISX for multiparametric CTC phenotyping. The ISX was used to establish an EpCAM–EGFR based CTC detection protocol. While EpCAM is the most commonly used biomarker for CTC detection, I included EGFR as an additional marker, in order to detect both epithelial CTCs and those under pEMT.

For comprehensive profiling of CTCs an extension of the staining panel was required in order to analyse the activation status of the EGFR–pathway (phospho–EGFR), the expression level of immune checkpoint markers (PD–L1 /–L2) and the response to radiotherapy (Figure 1). The response to radiotherapy was measured by quantifying the amount of DNA double–strand breaks, which can be detected through the amount of the phosphorylated form of the histone 2a variant (γH2AX–foci).

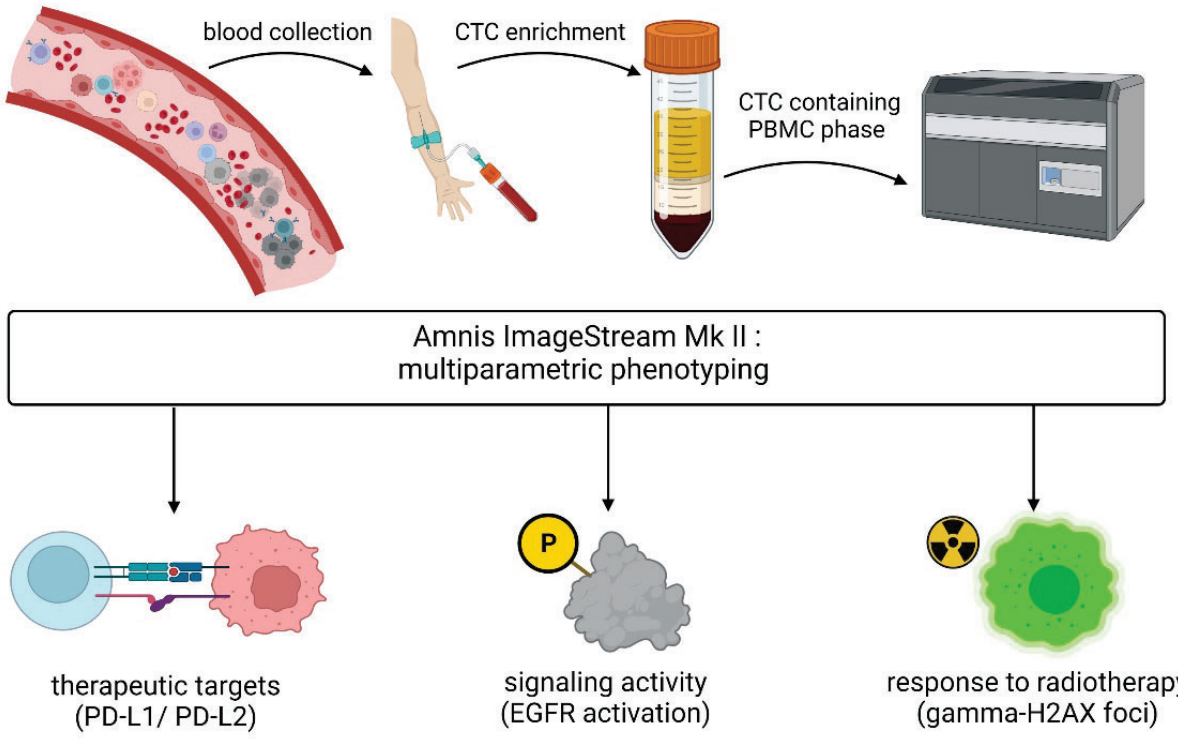

Figure 1: Overview of the CTC enrichment procedure and markers of interest. From Staudte et al. [12] Copyright © 2022 The Authors. Generated with BioRender.com.

In a pilot study, the EpCAM–EGFR based PD–L1 /–L2 CTC assay was applied to blood samples of patients diagnosed with either HNSCC or breast cancer (BC). The results

have proven the suitability of my ISX–based assay to characterize CTCs in patient blood samples. Since the patient cohort of the pilot trial was heterogeneous in terms of tumour entity, stage and treatment, a subsequent study was launched to evaluate the CTC assay in a more homogeneous patient cohort. Here, the focus was set on patients with recurrent /metastatic (R/M) HNSCC treated with an anti–PD–1 inhibitor, Nivolumab or Pembrolizumab. The study aimed at identifying the CTC cut–off value correlated with poor clinical outcome for patients with R/M HNSCC and determining whether PD–L1 /–L2^{positive} CTCs can predict response to ICI.

2 Methods

2.1 Cell lines

Human cell lines used for spiking experiments were selected according to their expression levels of EpCAM–EGFR and PD–L1 /–L2 (Table 1). The colorectal cancer cell line SW620 (ATCC® CCL 227™, purchased from ATCC, Manassas, VA; USA) and a HNSCC cell line UD–SCC–4 (University of Düsseldorf, NRW, Germany) were used to determine the sensitivity of the CTC assay. Both have been proven to be least sensitive to healthy donor´s allogenic immune response. Compensation matrix and laser power were set using the BC cell line MDA–MB–231 (ATCC® HTB–26™, purchased from ATCC) and HNSCC cell line SCC–25 (ATCC®, CRL-1628™, purchased from ATCC), respectively. Due to their EMT–like phenotype, the expression intensity of EpCAM–EGFR in MDA–MB–231 cells is comparable to the intensity expected on patient–derived CTCs. Combination of both cell lines enabled the establishment of PD–L1 /PD–L2 staining protocols. In addition, the HNSCC cell lines UM–(University of Michigan, IL, USA) –SCC–22B, a gift from T.K. Hoffmann (University of Ulm, BW, Germany [13]) and FaDu (ATCC®HTB–43™, purchased from ATCC) were used to establish the staining protocols for the analysis of phospho–EGFR and γH2AX, respectively. In previous projects, it was shown that UM–SCC–22B cells highly express EGFR. All cell cultures were tested negative for mycoplasma contamination and maintained in a humidified chamber at 37°C and 5% CO_2. Each cell line required a specific culture medium as mentioned in Table 2.

Table 1: Expression intensities of targets of interest. *Own presentation Staudte et al., unpublished data.*

Cell lines	EpCAM	EGFR	PD–L1	PD–L2	Sensitivity to HD immune response
SW620	high	no	no	no	low
UD–SCC–4	high	high	no	no	low
MDA–MB–231	low	moderate	moderate	low	moderate
SCC–25	high	high	low	moderate	moderate
FaDu	moderate	moderate	moderate	moderate	high
UM–SCC–22B	high	high	no	no	not tested

HD – healthy donor

2.2 Blood collection

The Ethics Committee of the Charité University Hospital approved both studies (EA1/152/10). After obtaining written informed consent, 10 ml blood from healthy donors (n=7) and patients were collected into ethylenediaminetetraacetic acid (EDTA) vacutainer tubes (BD, NJ, USA). For both studies, patients with either locally advanced (LA) or R/M HNSCC (LA: n=9; R/M: n=54) and BC (n=8) were enrolled. Blood was drawn before the start of therapy (T0) and at two time points during treatment (T1 /T2). The blood collection was performed prior the administration of therapy.

Table 2: Overview of the different cell culture media compositions per cell line. From Staudte et al. [12] Copyright © 2022 The Authors.

Cell line	Ingredients	Final conc.	Company / Order number
FaDu	MEM Medium	1x	LifeTechnologies,
UD–SCC–4			cat. no.: 31095052
UM–SCC–22B	Fetal calf serum (FCS)	10%	Life Technologies,
			cat. no.: 10270-106
	Non–essential amino	1x	LifeTechnologies,
	Acids (NEAA)		cat. no.: 11140035
MDA–MB–231	Advanced DMEM /F12	1x	ThermoFisher,
			cat. no.: 12634010
	FCS	10%	Life Technologies,
			cat. no.: 10270-106
	L–Glutamine	2mM	ThermoFisher,
			cat. no.: 25030149
SW620	RPMI Medium 1640	1x	LifeTechnologies
			cat. no.: 21875-034
	FCS	20%	Life Technologies,
			cat. no.: 10270-106
	L–Glutamine	2mM	ThermoFisher,
			cat. no.: 25030149
	Penicillin /Streptomycin	1%	Fisher BioReagent,
			cat. no.: BP2959-50
SCC–25	DMEM /F12 + GlutaMax	1x	ThermoFisher,
			cat. no.: 31331093
	FCS	10%	Life Technologies,
			cat. no.: 10270-106
	L–Glutamine	2mM	ThermoFisher,
			cat. no.: 25030149
	Penicillin /Streptomycin	1%	Fisher BioReagent,
			cat. no.: BP2959-50
	HEPES	15mM	sigma,
			cat. no.: H4034-100g

2.3 Blood sample processing for CTC detection

Blood samples were processed earliest 30 min or latest four hours after collection. CTCs were enriched by performing a CD45 depletion, which reduced the amount of peripheral mononuclear blood cells (PBMC). For this, the RosetteSep™ Human CD45 Depletion Cocktail (Stemcell Technologies, Vancouver, BC, Canada) was used according to the manufacturer´s instruction for 50 ml standard tubes. Briefly, 50 µl of CD45 depletion cocktail was added per 1 ml of blood, mixed and incubated for 20 min at room temperature (RT). Blood was diluted with an equal volume of washing buffer, composed of Dulbecco´s Phosphate Buffered Saline (PBS; Gibco™, Waltham, MA, USA, cat. No. 14190–094) and 2% Fetal Bovine Serum (FBS; Gibco™, cat. No. 10270–106). Diluted blood was transferred onto a layer of 15 ml Ficoll Paque™ PLUS (Cytiva, Marlborough, MA, USA) without mixing the two phases. The sample was centrifuged at 1200 xg for 20 min at RT with the break off. PBMC interphase was harvested by using a transfer pipette, washed twice with PBS /2% FBS and centrifuged at 300 xg for 10 min at RT with low break. After washing, cells were transferred into a 5 ml FACS tube for subsequent staining.

2.4 Immune fluorescence (IF) staining for multiparametric CTC phenotyping

The following fluorescence–conjugated antibodies were used for IF staining to perform multiparametric CTC phenotyping: AlexaFluor® 488 anti–human CD326 (EpCAM) Antibody (Biolegend, San Diego, CA, USA, cat. No. 324210, clone: 9C4, 1:100); AlexaFluor® 488 anti–human EGFR Antibody (Biolegend, cat. No. 352908, clone: AY13, 1:100); AlexaFluor® 647 anti–human CD45 Antibody (Biolegend, cat. No. 304018, clone: HI30, 1:50); PE anti–human CD274 (B7H1, PD–L1) Antibody (Biolegend, cat. No. 393608, clone: MIH2, 1:20) and PE–Vio® 770 anti–human CD273 (PD–L2) REAfinity™ Antibody (Miltenyi, Bergisch Gladbach, NRW, Germany, cat. No.130–116–565, clone: REA985, 1:50). All centrifugation steps were performed at 300 xg, for 5 min at 4°C and after adding the fluorescence–labelled antibodies, samples were kept protected from light exposure and at 4°C.

After an initial washing step with PBS /10% FBS, cells were suspended in 100 µl PBS /10% FBS, 10 µl FcR Blocking reagent (Miltenyi, cat. No. 130–059–901, 1:11) was added and samples were incubated for 10 min at 4°C. Fluorescence–labelled antibodies were added and incubated for 15 min at 4°C, followed by a washing step with

PBS /10% FBS. This was followed either by fixation with 4% formaldehyde (Carl Roth, BW, Germany, cat. No. 4979.1, 1:9.25 dilution of 37% formaldehyde) for 15 min at 4°C or intracellular staining, including phosphorylated EGFR (phospho–EGFR) and γH2AX.

To analyse the activation status of EGFR (phospho–EGFR) or the response to irradiation (γH2AX), cells were treated with 100 ng/mL EGF (Invitrogen, Waltham, MA, USA, cat. No. PHG0315) for 10 min at 37°C and 5% CO_2 and /or irradiated with 2 Gray (Gy), respectively. After irradiation, cells were cultured for 1h under normal conditions, followed by 5 min EDTA–trypsin incubation to harvest the cells. Following the modified protocol of Durdik et al. [14] extracellularly stained cells were washed with ice–cold PBS, fixed with 1 ml 3% formaldehyde for 10 min, washed with PBS and stored in 70% ethanol overnight at -20°C. On the next day, cells were permeabilized with PBS containing 1% bovine serum albumin (BSA) and 0.1% Triton X–100 (Th. Geyer, Renningen, BW, Germany) for 30 min at RT. The following premixed primary or fluorescence–conjugated antibodies were added and samples were incubated for 2h at RT: Phospho–EGF Receptor (Tyr1068) (D7A5) XP® Rabbit mAb (Cell Signaling, Danvers, MA, USA, cat. No. 3777S, 1:1600) or AlexaFluor® 647 anti H2A.X Phospho–Ser139 Antibody (Biolegend, cat. No. 613408, clone: 2F3, 1.25 µg/mL). For secondary staining, antibody Texas Red–labelled goat anti–Rabbit IgG (Invitrogen, cat. No. T–2767, 4 µg/mL) was diluted in PBS/ 1% BSA/ 0.1% Triton X–100 and incubated for 1h at RT after an additional washing step with PBS.

After extracellular and intracellular staining, cells were washed with PBS and counterstained with Hoechst 33342 (LifeTechnologies, Waltham, MA, USA, cat. No. H1399, 2 ng/mL) for 20 min. The stained cells had to be transferred into a 1.5 ml tube, because this is the format compatible with the ISX. Respective isotype controls for each antibody were used in order to determine unspecific background signal and to set the gates for marker–positivity.

2.5 Imaging flow cytometry analysis

The Amnis® ImageStream®X Mk II (ISX) is an imaging flow cytometer, which can be equipped with up to six lasers, thereby allowing multicolour analysis. Lasers at 405 nm, 488 nm, 561 nm and 642 nm and the INSPIRE™ Software (version 201.1.0.765) were used for sample acquisition. The 40X objective resulted in high–quality images of the cells and allowed detailed analysis of both extra– and intracellular stained targets. The fluidics

were set to low speed to maintain high sensitivity, resulting in a total acquisition time of 30 min per 30 µl sample volume. When performing γH2AX staining only, the 60X magnification and the EDF were preferably used for a better distinction of single foci inside the nuclei.

To set the laser power and generate the required compensation matrix, a mixture of MDA–MB–231 /SCC–25 cells and healthy donor derived PBMCs was stained for the above–mentioned antibodies alone or in combination. For each new antibody batch, a new matrix was generated. The final laser settings are listed in Table 3.

Table 3: **Summary of the laser settings and assignment of the individual channels.** From Staudte et al. [12] Copyright © 2022 The Authors.

Laser (nm)	Target	Fluorophore	Channel	Laser power (mW)
405	Hoechst 33342		7	30
488	EpCAM–EGFR	AF488	2	100
561	PD–L1	PE	3	200
561	phospho–EGFR	TexasRed	4	200
561	PD–L2	PE–Vio770	6	200
642	CD45 /γH2AX	AF647	11	150 /130
642	CD45	APC /Fire	12	130
782	SCC		12	0.9
bright field			1 and 9	

nm – nanometer; mW – milliwatt; AF – Alexa Fluor® ; PE – Phycoerythrin, UV – ultraviolet, APC - Allophycocyanin

2.6 Spiking experiments

In order to determine sensitivity and specificity of the ISX–based CTC assay, spiking experiments were performed with SW620 and UD–SCC–4 cells. Several cell lines have been tested, demonstrating that these two cells lines were least sensitive to endogenous immune response by natural killer cells of the healthy donor´s immune system (data not shown /published). Recovery frequencies of the SW620 cell line were published by other

groups and indicate an expected recovery rate [15]. Cells were harvested by trypsin–EDTA treatment at a confluence of 90%, counted using a Neubauer counting chamber and diluted in 1 ml RPMI1640 to get absolute cell numbers of 500, 50 or 5 cells. Blood of a healthy donor was drawn and incubated for 30 min at RT before used for spiking. The 1 ml of prepared cell suspensions was either added to 4 ml blood (blood–spiked sample) or 4 ml culture medium (reference sample). The reference sample was used to calculate the recovery frequency of my assay in the blood–spiked samples. Blood–spiked samples were processed following the RosetteSep™ Human CD45 Depletion Cocktail kit as mentioned above. The isolated PBMC /CTC interphase from the blood–spiked samples and reference samples were stained for EpCAM–EGFR, CD45 and Hoechst. Spiking experiments were performed in biological triplicates for robust statistical analysis.

2.7 Statistical analysis

Results obtained from spiking experiments were analysed using MS Excel 2016. IBM SPSS Statistics (version 27.0.0.0) was used to perform statistical analysis of the clinical data in correlation with the results of the CTC analysis. Receiver operating curve (ROC) analysis was used to identify the cut–off value of CTC positivity prognostic for disease progression. Kaplan–Meier curves were used for time–to–event analysis for both overall survival (OS) and progression free survival (PFS) and tested by log–rank test. P-values of ≤ 0.05 were considered as statistically significant.

3 Results

3.1 Establishment of a multiparametric CTC phenotyping assay

EpCAM is the most prominent tumour–marker for epithelial solid malignancies and predominantly used for CTC detection [16]. However, EpCAM was shown to be downregulated in squamous cell carcinomas [17], whereas EGFR is frequently overexpressed in these tumours. In addition, EpCAM is downregulated or even absent in tumour cells being under EMT [16], whereas EGFR is often still present. Thus, I hypothesized that using both tumour–markers may improve the sensitivity of my assay [16]. After tumour–marker identification, the optimal antibody concentrations for EpCAM, EGFR and CD45 were determined, followed by the establishment of the subsequent gating strategy for CTC detection. Initially, speedbeads and cell debris were excluded based on their different size, being either smaller or significantly larger than single cells /cluster, respectively. Nucleated cells were further classified according to their CD45–AF647 or EpCAM–EGFR–AF488 signal intensity, in order to distinguish between CD45^{positive} leukocytes and EpCAM–EGFR expressing tumour cells (Figure 2). To eliminate unspecific background signal, isotype controls were utilized and gating was performed accordingly.

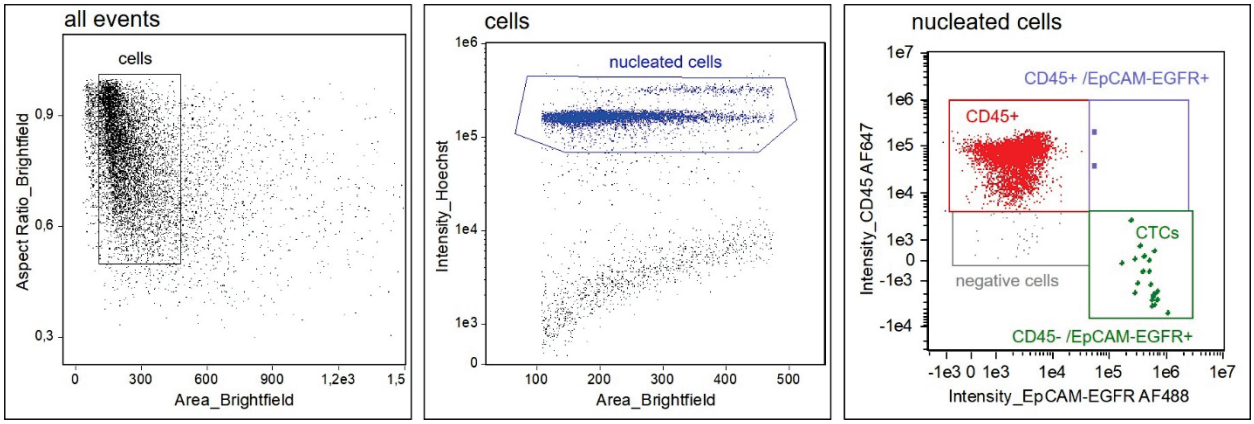

Figure 2: Gating strategy for CTC detection. From left to right: speedbeads and debris were excluded, nucleated cells were used for subsequent analysis of their CD45–AF647 and /or EpCAM–EGFR–AF488 signal. CTCs were classified as EpCAM–EGFR^{positive} /CD45^{negative} / Hoechst^{positive} and showed heterogeneous EpCAM–EGFR staining intensity. Clusters of leukocytes and CTCs are detectable in the upper right square. From Staudte et al. [12] Copyright © 2022 The Authors.

3.2 Evaluation of assay sensitivity and specificity

Spiking experiments with human cell lines were performed to investigate the sensitivity and specificity of the established CTC assay. Sensitivity was determined by the recovery frequencies (RF) of 5, 50 and 500 spiked cells. The RF was calculated by dividing the number of recovered tumour cells in the "blood–spiked sample" by the number of the detected tumour cells in the corresponding "reference sample" and multiplied by 100. A median RF of 73% with a correlation of R^2=0.97 was achieved for the biological triplicates of all three cell counts for SW620 cells (Figure 3A). Comparable results were observed for UD–SCC–4, yielding in a lower recovery frequency of 50% but good correlation of R^2=0.92 (Figure 3B). By analysing each measured event, differentiation of tumour cells (EpCAM–EGFR^{positive} /CD45^{negative} /Hoechst^{positive}) and leukocytes (EpCAM–EGFR^{negative} / CD45^{positive} /Hoechst^{positive}) or clusters of tumour cells and leukocytes (Figure 3C) was achieved.

In a blinded analysis of blood samples (n=11) from seven healthy donors, CTC assay specificity was evaluated. A positive control composed of UD–SCC–4 cells being spiked in a blood sample of a healthy donor prior blinding and processing, was processed and measured in parallel with healthy donor samples. Isolation, staining and analysis was done as described in the methods and materials section (6.3 and 6.4). Without the implementation of a cut–off, one of 11 (9%) samples was tested positive for two EpCAM–EGFR^{positive} cells, resulting in a 91% specificity. However, with the application of the cut–off value of ≥ 3 CTCs /7.5ml blood, which was associated with a poor clinical outcome in colorectal cancer [10] my assay demonstrated a specificity of 100%.

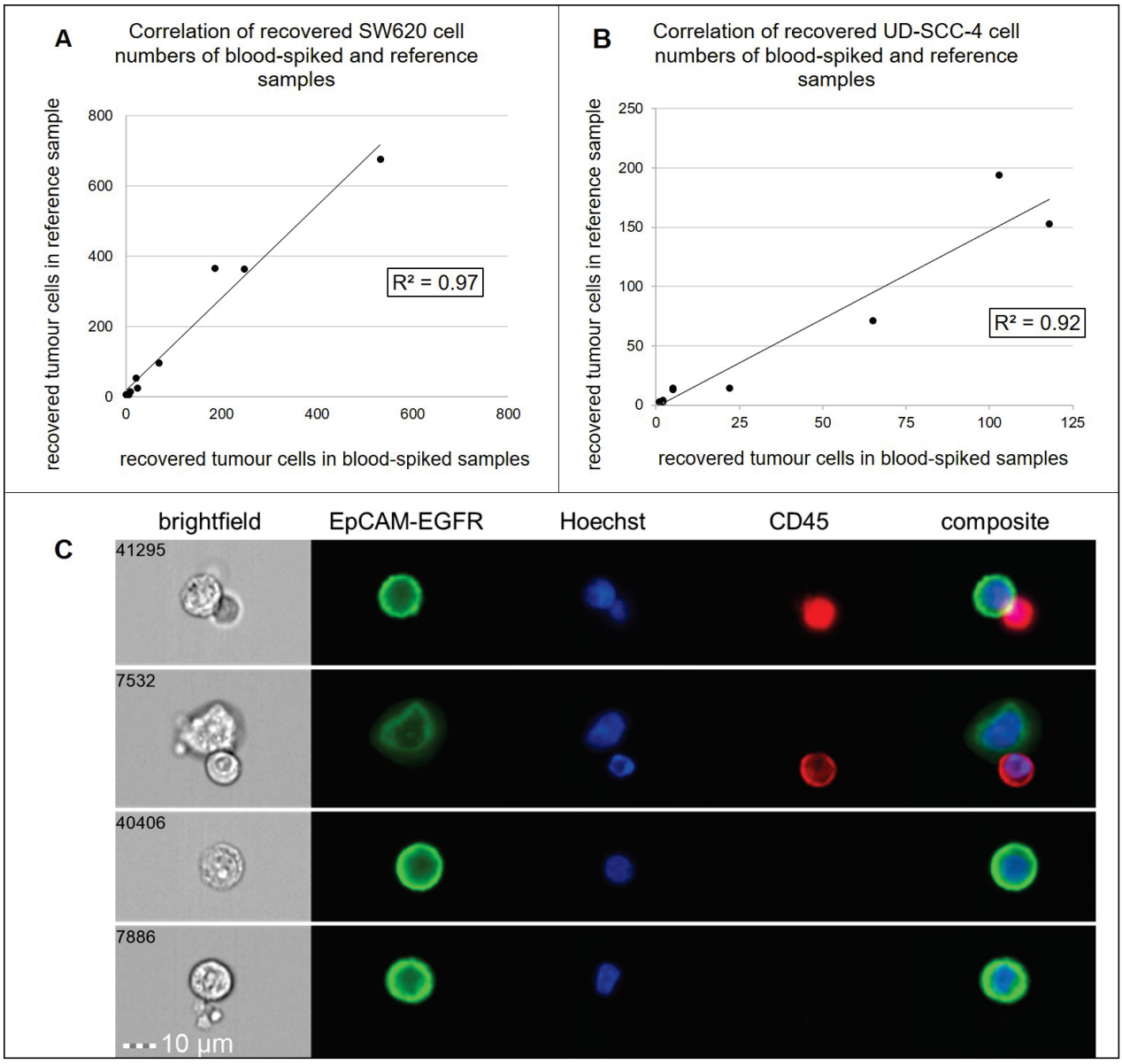

Figure 3: Recovery rates of spiking experiments and exemplary microscopic images of retrieved tumour cells. Scatter plots depict the correlation of median recovered tumour cells with the respective reference sample of (A) SW620 and (B) UD–SCC–4. (C) Representative images of recovered single tumour cells and clusters with leukocytes ($CD45^{positive}$). Modified from Staudte et al. [12] Copyright © 2022 The Authors.

3.3 Extension of the staining panel for multiparametric phenotyping

Important therapeutic targets for many solid tumours such as EGFR and the immune checkpoint molecules PD–L1 /–L2 may represent promising prognostic biomarkers on CTCs. Additionally, quantification of the γH2AX–foci, which occur on DNA double–strand breaks, might be suitable as a prognostic marker for radioresistance [14]. Rapid removal of formed γH2AX foci after radiation is indicative for efficient DNA repair mechanism and

thus for radioresistance. The combination of γH2AX and PD–L1 /–L2 staining is of special interest, because radiotherapy has a modulating impact on the patient's immune system [18]. Therefore, these targets were included in the established CTC assay and working concentration was determined for each marker individually to allow discrimination between the negative (unstained, isotype, untreated) and positive (targeted antibody and treated) population per target (Figure 4). In order to establish the phospho–EGFR staining, cells were treated with EGF prior staining to induce an activation of EGFR signalling and thereby enable its detection. This allowed a separation of untreated (phospho–EGFR^{negative}) and treated (phospho–EGFR^{positive}) cells (Figure 4A). The establishment of the staining for PD–L1 /–L2 was based on the MDA–MB–231 (PD–L1^{high} /PD–L2^{low}) and SCC–25 (PD–L1^{low} /PD–L2^{moderate}) cell lines (Figure 4B-C). FaDu cells were used to establish the staining for γH2AX foci analysis and were either left untreated, in order to get the basal amount of γH2AX foci, or irradiated with a single dose of either 2 Gy or 10 Gy, which in turn leads to an increase in foci number. Sample analysis revealed a clear dose–dependent staining intensity (Figure 4D). Finally, EGF–treated and irradiated FaDu cells were spiked into healthy donor blood, enriched and stained with the combinatory antibody panel, confirming the suitability of the CTC assay for simultaneous analysis of oncogenic signaling, therapeutic target expression and therapy response.

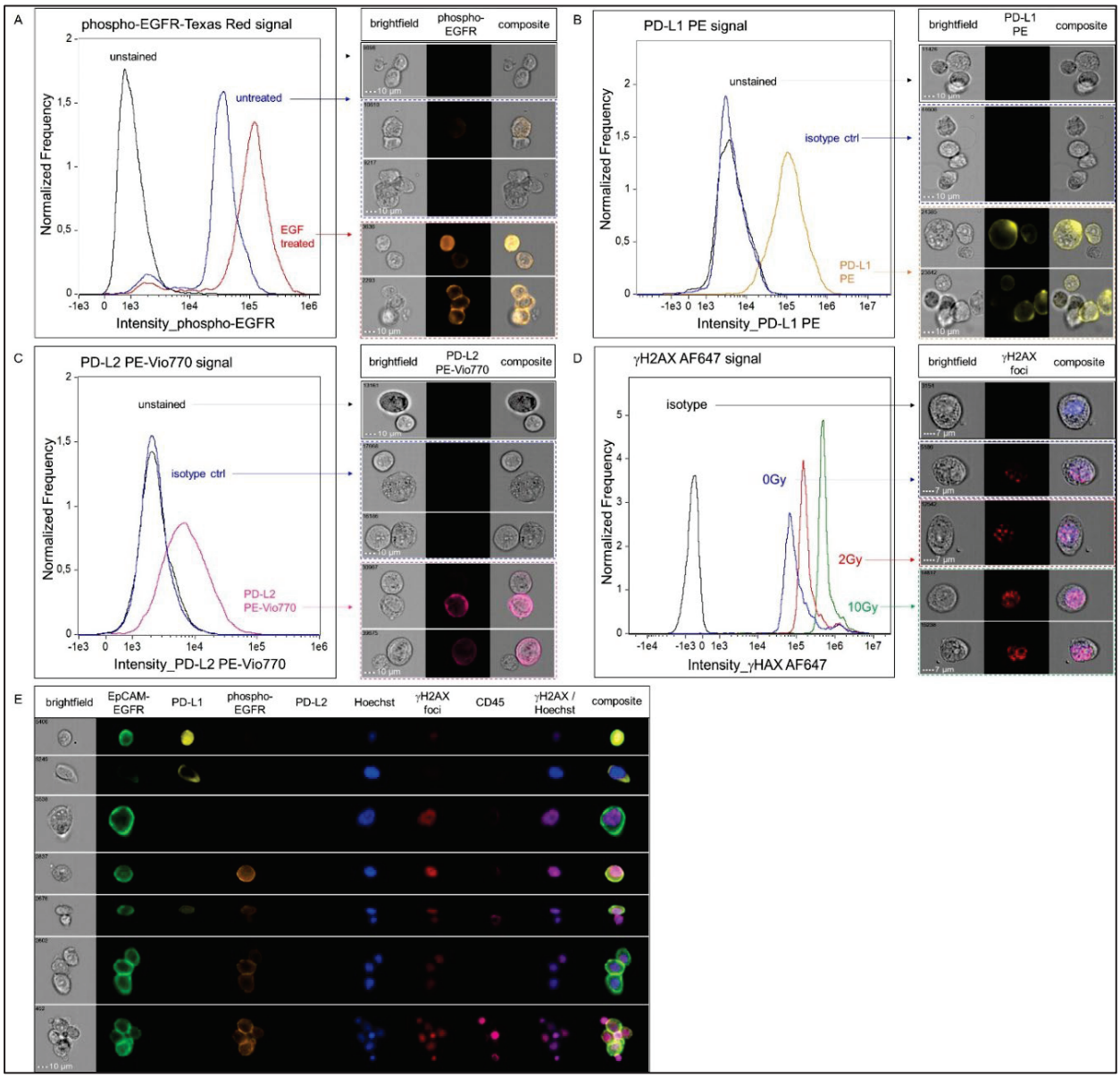

Figure 4: IF staining for the analysis of EGFR activation (phospho–EGFR), expression of therapeutic targets (PD–L1 /–L2) and response to radiotherapy (γH2AX foci). (A) Representative images of EGF–treated (phospho–EGFR^{positive}) and untreated (phospho–EGFR^{negative}) UM–SCC–22B cells. The histogram displays the mean fluorescence intensities (MFI) for unstained cells (black), untreated (blue) and EGF-treated cells (orange). Images showing the staining for extracellular (B) PD–L1 on MDA–MB–231 cells and (C) PD–L2 on SCC–25 cells. Histograms display the MFI for unstained (black), isotype control (blue) and (B) PD–L1 (yellow) or (C) PD–L2 (pink), respectively. (D) Representative images of γH2AX staining of irradiated FaDu cells, demonstrating a dose–dependent increase of the MFI. The histogram displays the intensities for isotype (black), untreated (blue), single dose of 2 Gy (red) and a single dose of 10 Gy (green). From Staudte et al. [12] Copyright © 2022 The Authors.

In order to quantify γH2AX foci in a semi–automated process, I developed a mask, based on the IDEAS default mask for spot counting. Samples irradiated with a high dose and a low dose were used to define different foci shapes and staining intensities (Figure 5). As shown in Figure 5, there is a relationship between number of foci and radiation dose administered.

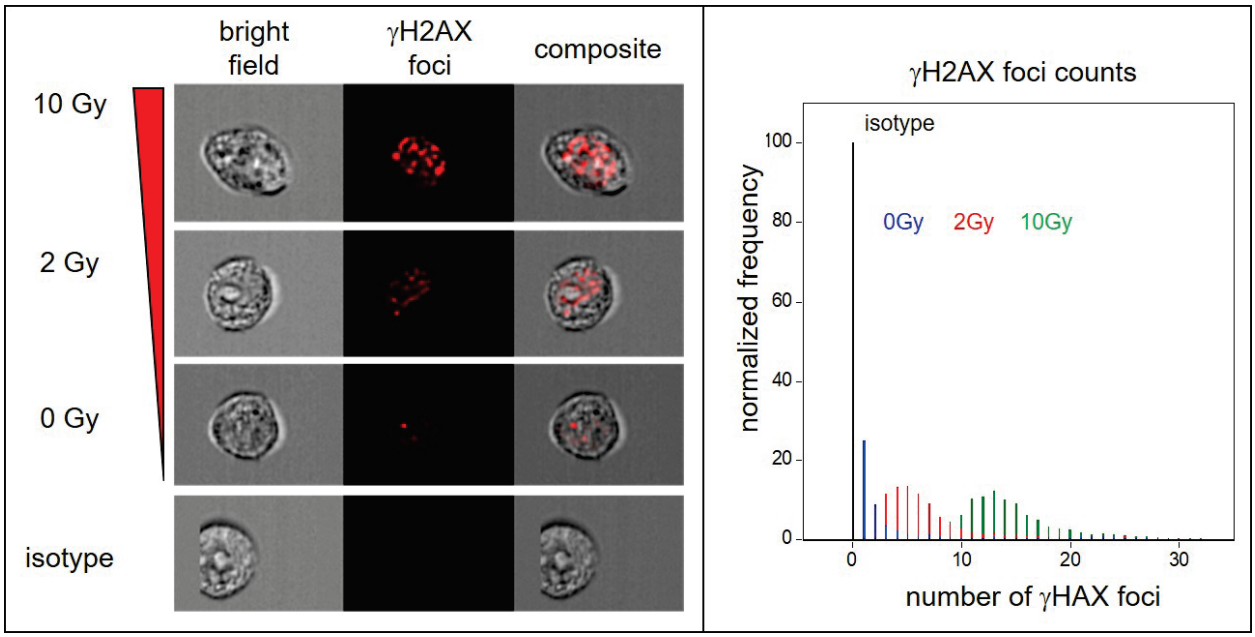

Figure 5: γH2AX foci quantification. Mask for automated foci counting was applied to data acquired from samples irradiated with increasing doses. A correlation between doses and number of counted γH2AX foci was observed. For data acquisition, the 60x magnification and the EDF module was used, in order to gain a higher in–depth resolution of the foci. Modified from Staudte et al. [12] Copyright © 2022 The Authors.

3.4 Pilot study as a proof of concept – Assessment of CTC numbers in patient blood samples

A pilot study was conducted to prove the suitability of the CTC assay for multiparametric phenotyping, including the analysis of PD–L1 /–L2. Blood from patients with either L/A or R/M HNSCC (n=16) and BC (n=8) was collected prior treatment (T0) and during therapy (T1) for CTC analysis. Characteristics of the patients enrolled in this pilot study are presented in Table 4.

Table 4: Characteristics of the patients included in the pilot CTC study. From Staudte et al. [12] Copyright © 2022 The Authors.

Characteristics		HNSCC	BC
Gender	female	4	8
	male	12	-
Age	female	70 (32-81)	48 (34-64)
Median (range)	male	69 (58-79)	-
Stage of disease n (%)	early stage	-	4 (50%)
	locally advanced (L/A)	1 (6%)	-
	recurrent/metastatic (R/M)	15 (94%)	4 (50%)
Tumour site n (%)	oral cavity	8 (50%)	
	oropharynx	3 (19%)	
	hypopharynx	3 (19%)	
	other/breast	2 (12)	8 (100%)
Metastatic sites n (%)	none	1 (0,06%)	4 (50%)
	regional	3 (25%)	3 (38%)
	distant	12 (75%)	1(12%)
$CTC^{positive}$ cases (≥ 3 CTCs /7.5ml) n (%)		7 (44%)	6 (75%)
	CTC numbers		
	median	15	14
	range	6-30	9-27
$PD–L1^{positive}$ cases n (%)		4 (57%)	4 (67%)
	$PD\text{-}L1^{positive}$ cells		
	median (n)	6	2
	range (n)	3-30	1-6
% of $PD–L1^{positive}$ CTCs in entire CTC	median (%)	100%	15%
population	range (%)	56%-100%	4%-25%

Applying the cut–off value of ≥ 3 CTCs /7.5ml blood, 7 /16 (44%) HNSCC patients were $CTC^{positive}$ at baseline, of which 4 patients presented with $PD–L1^{positive}$ CTCs. The amount of $PD–L1^{positive}$ CTCs within this cohort ranged from 56%–100%, emphasising the heterogeneity of the CTC population. Within the BC cohort, 6 /8 (75%) patients were tested $CTC^{positive}$, of which 4 cases contained 4%–25% $PD–L1^{positive}$ CTCs. The expression levels of PD–L1 /–L2 varied within individual samples. Representative images of detected CTCs are shown in Figure 6.

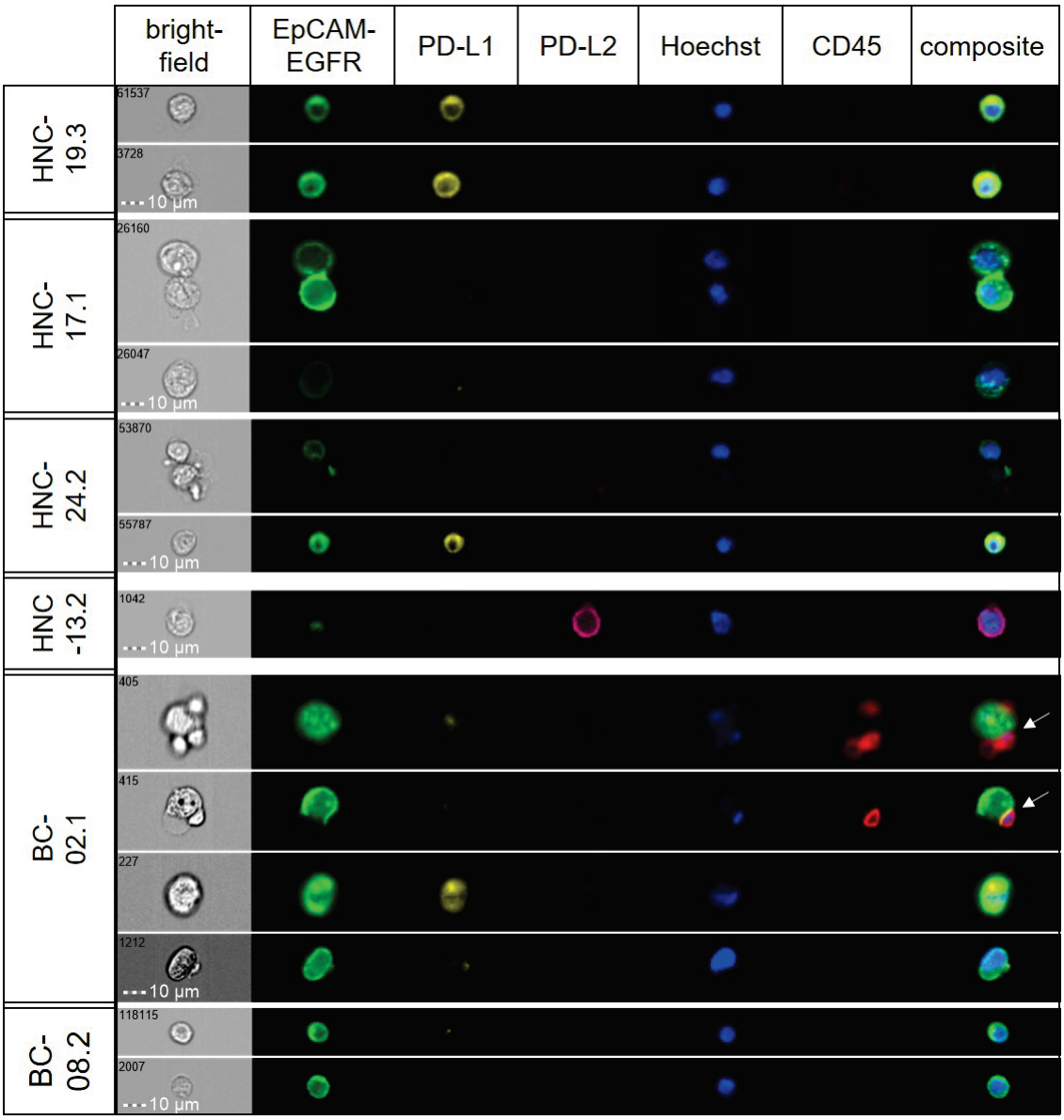

Figure 6: Representative images of CTCs depicting the high heterogeneity of PD–L1 /–L2 expression within individual samples and the overall cohort. Clusters of CTCs (HNC–17.1) and clusters of CTCs with leukocytes (BC–02.1; white arrows) were observed. From Staudte et al. [12] Copyright © 2022 The Authors.

With respect to tumour heterogeneity and the diagnostic potential of CTCs, a correlation analysis of the PD–L1 expression level on tumour tissue and CTCs was performed. Tissue samples were available from 7 /13 $CTC^{positive}$ cases (≥ 3 CTC; HNSCC n=5, BC n=2). A weak correlation (R^2 =0.22) of PD–L1 positivity in tumour tissue and corresponding CTCs was observed in 4 /7 (57%) cases. In tumour samples from two patients, a tumour proportion score (TPS) of 5% and 70% was detected whereas 100% of the CTCs expressed PD–L1. The other two concordant cases were tested $PD\text{-}L1^{negative}$

in both specimens. The median time span between tissue collection and blood draw for CTC analysis was 4.6 months (range: 0.4–19 months, Table 5).

Table 5: Time span between tumour sample collection used for TPS determination and PD–L1 expression analysis on CTCs. For all CTC^{positive} cases (≥ 3 CTCs/ 7.5ml), results of TPS and CTC analysis for PD–L1 expression are shown as well as the time between sample collection. Concordant cases are highlighted in green. From Staudte et al. [12] Copyright © 2022 The Authors.

Pat.ID	Tumour site	PD–L1^{positive} cells in tumour tissue (TPS %)	PD–L1^{positive} CTCs (%)	Time between tumour and liquid biopsy (months)
BC–003	breast	0	8	0.4
BC–006	breast	0	20	1
HNC–012	oral cavity	70	100	0.4
HNC–018	oral cavity	0	0	19
HNC–019	oral cavity	0	45	5
HNC–020	hypopharynx	5	100	12
HNC–026	hypopharynx	0	0	15

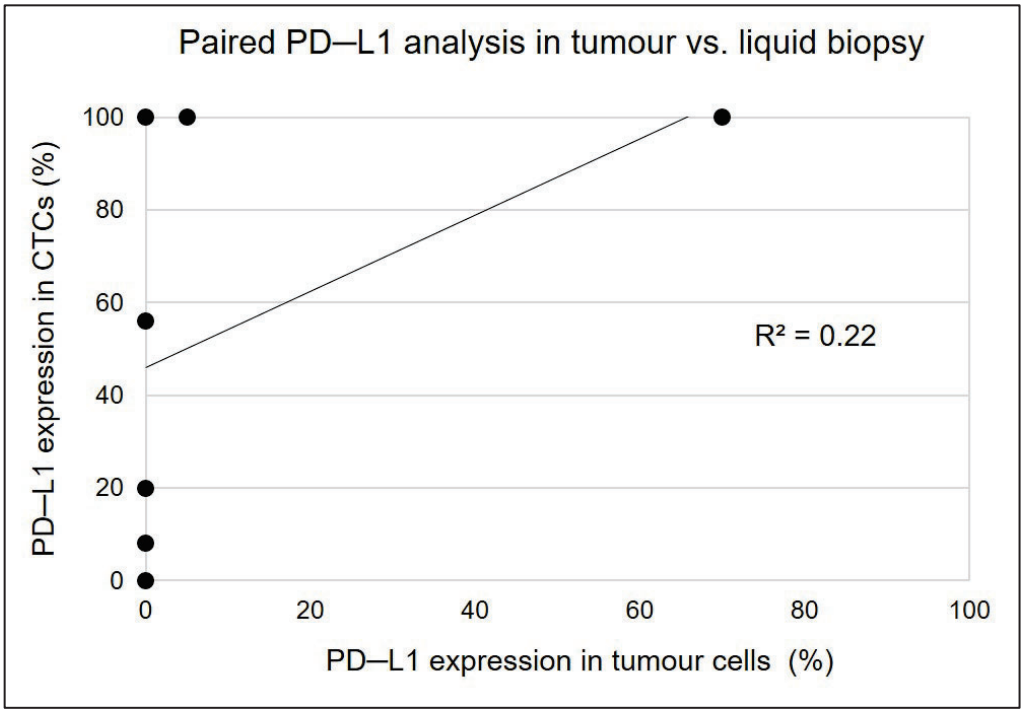

Figure 7: Paired analysis of PD–L1 status of tumour tissue and liquid biopsy. CTC^{positive} (≥ 3 CTCs /7.5ml) cases were used for paired analysis. A concordance was seen in four HNSCC cases. From Staudte et al. [12] Copyright © 2022 The Authors.

3.5 Clinical trial (ICI CTC Study) investigating the prognostic and predictive value of PD–L1^{positive} CTCs in R/M HNSCC

The two ICIs targeting PD–1, Nivolumab and Pembrolizumab, have obtained clinical approval for R/M HNSCC in 2016 and 2019, respectively [19]. Both antibodies increased survival of patients with PD–L1^{positive} tumours, compared to standard of care treatment with chemotherapy [20, 21]. Assessment of PD–L1 expression in tumour tissue is not required to start Nivolumab treatment, whereas a combined positivity score (CPS) of ≥ 1 is a prerequisite for Pembrolizumab therapy.The CPS is composed of the amount of PD–L1^{positive} tumour cells (TPS) and PD–L1^{positive} immune cells (immune cells, IC) within the tumour tissue. Although the criterion of CPS ≥ 1 is predictive for a response to ICI in R/M HNSCC, there is still a high amount of patients not responding to ICI. On the other hand, there are also patients who respond to ICI therapy despite the absence of PD–L1 expression [4]. This may suggest that another biomarker, such as the immune checkpoint status of CTCs, could be favourable to improve the identification of patients who would benefit from this treatment.

Thus, a prospective observational trial aiming at investigating the prognostic and predictive value of PD–L1^{positive} CTCs in R/M HNSCC patients by applying the established ISX–CTC assay was conducted. Blood samples were collected at three time points: prior to treatment initiation (T0) and preceding the third (T1) and fifth (T2) cycles for Pembrolizumab, or the third (T1) and seventh (T2) cycles for Nivolumab. Given the different treatment schedules, with Nivolumab administered every two weeks and Pembrolizumab every three weeks, the T2 time point was designated to represent twelve weeks of treatment, regardless of the specific cycle of ICI therapy. Patients with R/M HNSCC enrolled for the pilot study have also been included into the analysis. Baseline patient characteristics are listed in Table 6. The cohort (n=54) is predominantly composed of male patients (83.3%) with a median age of 70 years at time point of R/M HNSCC diagnosis. The HPV status, smoking history and amount of alcohol consumption were not analysed for this study. The PD–L1 status of the tumour tissue was considered in order to correlate it with the PD–L1 status of the CTCs.

Table 6: Characteristics of R/M HNSCC patients (n=54) enrolled for the ICI CTC Study. *Own presentation S. Staudte, unpublished data*.

Characteristics		n (%)	Median (min–max)
Gender	*Female*	9 (16.7%)	
	Male	45 (83.3%)	
Age	*Female*		67 (33–86)
	Male		70 (42–94)
Survival status 05/2023	*Alive*	16 (29.6%)	
	Deceased	38 (70.4%)	
Tumour site	*Oropharynx*	15 (27.8%)	
	Hypopharynx	5 (9.3%)	
	Larynx	7 (13.0%)	
	Oral cavity	26 (48.1%)	
	Oro-/Hypopharynx	1 (1.9%)	
Site of progression	*Locally recurrent*	21 (38.9%)	
	Distant metastasis	33 (61.1%)	
Staging at first diagnosis	*0*	1 (1.9%)	
	I	3 (5.9%)	
	II	5 (9.3%)	
	III	13 (24.1%)	
	IVA	28 (51.9%)	
	IVB	2 (3.7%)	
	IVC	2 (3.7%)	
Treatment	*Pembrolizumab mono*	32 (59.3%)	
	Nivolumab mono	7 (12.9%)	
	EXTREME	9 (16.7%)	
	ICI+CTx	2 (3.7%)	
	other	4 (7.4%)	
Best response determined between T0 and T2	*CR*	3 (5.6%)	
	PR	7 (13.0%)	
	SD	8 (14.8%)	
	PD	36 (66.7%)	

CTx – chemotherapy; EXTREME – consisting of a combination of fluorouracil [5-FU] /platinum–based chemotherapy and cetuximab, an EGFR-inhibitor; MTX – Methotrexat. CR – complete remission; PR – partial remission; SD – stable disease, PD – progressed disease.

Prior to treatment application, blood was collected from 54 patients presenting with R/M HNSCC, either locally recurrent (n=21; 38.9%) and /or with distant metastasis (n=33; 61.1%). At T1, blood from only 44 patients could be collected, because health

condition of one patient drastically reduced, five study participants demonstrated with rapid cancer progression enforcing a change in treatment regimen, one died and three stopped treatment for other reasons. Blood specimen of 31 patients were available at T2, since 10 patients deceased and three experienced disease progression. As long as no earlier intervention was needed computer tomography /magnetic resonance imaging for response evaluation was performed after 12 weeks of therapy. Patients who were diagnosed with stable disease, partial remission or complete remission were classified as disease control group (DC; n=18; 33.3%). All other patients presented with either mixed response or progressing disease (PD; n=36; 66.7%). Tumour tissue for CPS determination was available from 43 of 54 (79.6%) cases. The median time between CPS determination of tissue biopsy and liquid biopsy analysis was 2.1 months (range: 0.1 – 15.7 months). Out of these 43 cases, blood samples of 20 patients (46.5%) were tested positive for at least 1 CTC /7.5ml and used for paired analysis (Figure 8). Paired analysis of CPS and PD–L1 status of the CTCs did not reveal any correlation (R^2=0.0173). In eight (40%) cases PD–L1 expression was detected in tissue and CTCs. For the 12 non–concordant cases (60%), PD–L1 expression was more frequently detected in the respective tissue samples. Lack of concordance could not be explained by a longer time span between biopsy sampling and blood analysis (median: 2.1 months; range: 0.5 – 10 months).

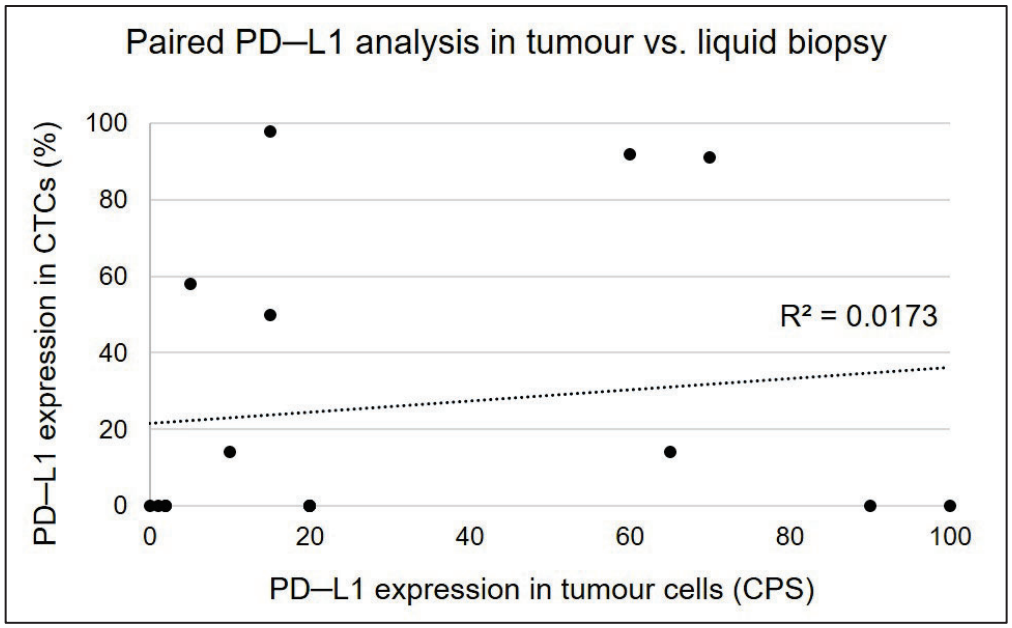

Figure 8: Paired analysis of tumour tissue and corresponding liquid biopsy for PD–L1 expression. In total, 20 cases were available for a paired PD–L1 analysis. Concordant PD–L1 status was observed in 40% (8/20) of the cases. Four had a CPS ≤ 2 and no PD–L1^{positive} CTCs,

while the remaining two cases had a CPS ≥ 60 and high PD–L1 expression (≥ 90%) on CTCs. *Own presentation S. Staudte, unpublished data.*

In the KEYNOTE–048 trial, it was shown that patients with a CPS ≥ 20 had a better response to Pembrolizumab treatment than the group with a CPS < 20 [22]. Therefore, we applied this cut–off value of CPS ≥ 20 to our cohort, resulting in a distribution of the cases as following: CPS ≥ 20 (n=23; 53.5 %) vs. CPS < 20 (n=20; 46.5 %). Kaplan–Meier analysis for overall survival (OS) and progression free survival (PFS) was performed. OS analysis showed no significant difference between the two groups. In contrast, PFS analysis revealed a significant better outcome for patients classified as CPS ≥ 20 (p<0.001; median: 6 months, range: 1 – 58.9 months vs. median: 2.5 months, range: 0.6 – 20.7 months, Figure 9).

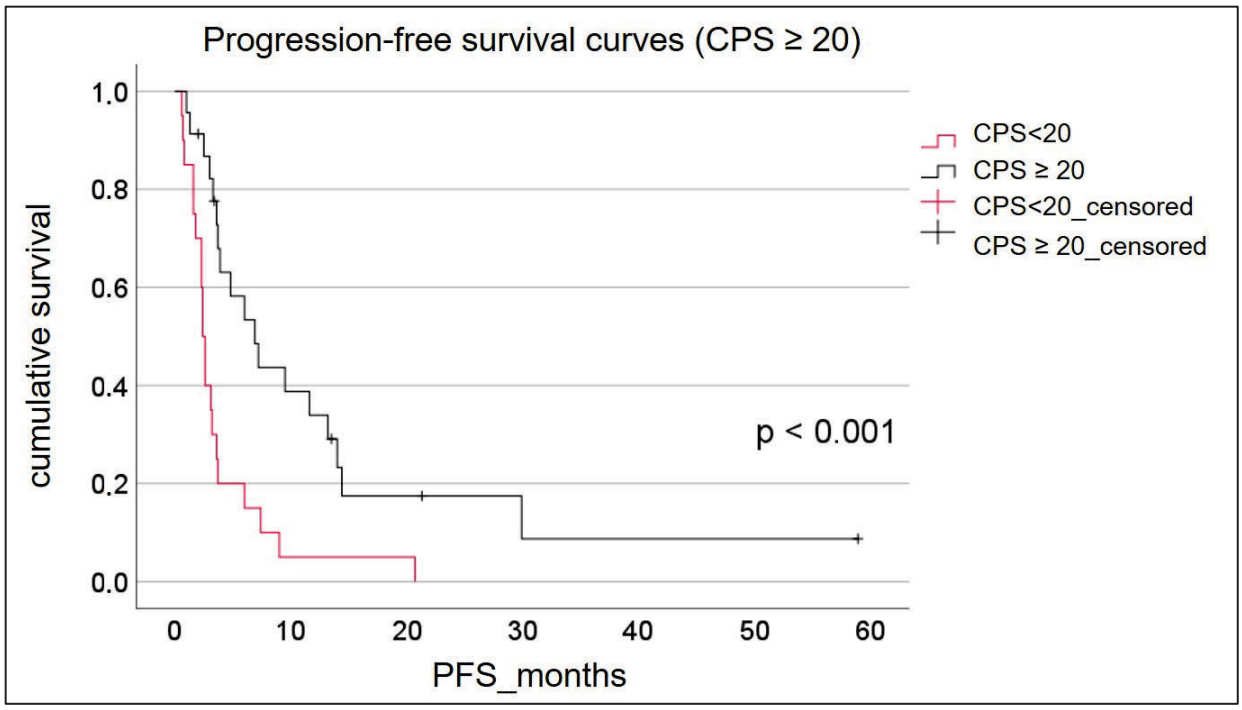

Figure 9: PFS of patients with CPS ≥ 20 compared to CPS < 20. Patients with CPS ≥ 20 (n=23) showed significantly (p<0.001) better PFS compared to the group classified as CPS < 20 (n=20). *Own presentation S. Staudte, unpublished data.*

ROC analysis was done to determine the cut–off value for CTC positivity. Survival status of all patients at six months after treatment initiation was used as separation variable. However, ROC analysis did not reveal a clinical relevant CTC cut–off value (Figure 10A). In addition, no correlation between response and CTC count was observed (Figure 10B).

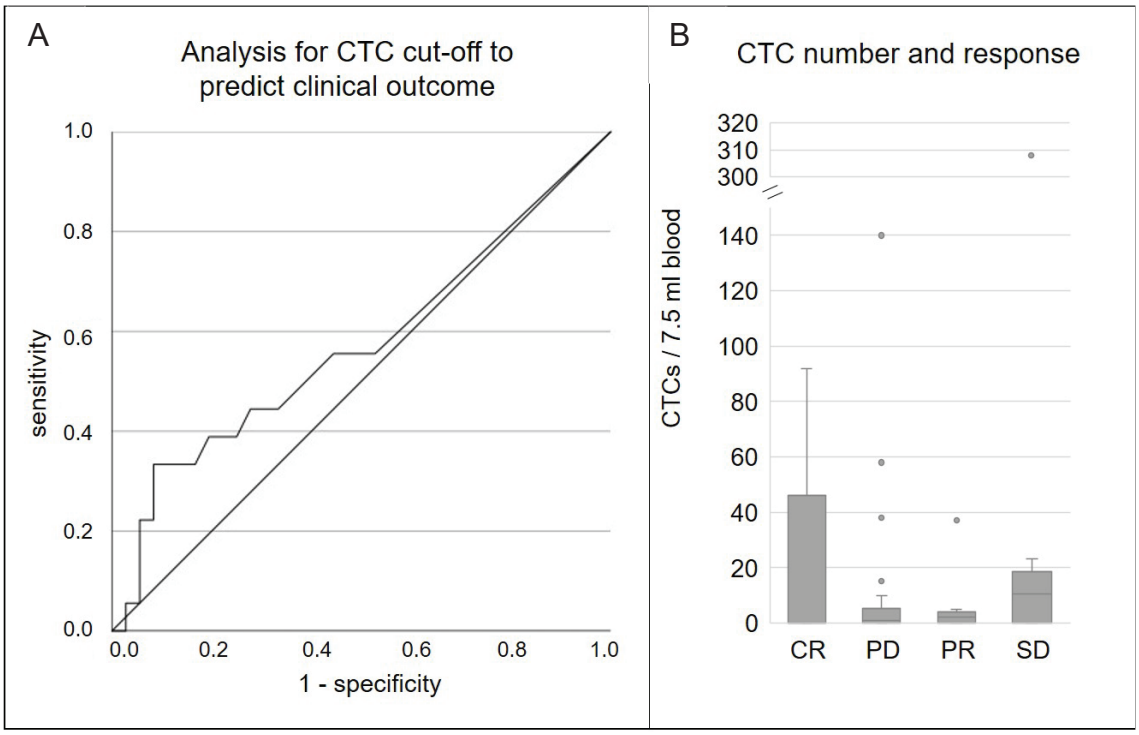

Figure 10: Cut–off for CTC positivity and CTC counts correlated to best response. ROC analysis did not reveal a relevant CTC count to predict clinical outcome, using patient´s survival status at six months after start of treatment as the separation variable. No correlation was observed between CTC count and best response, determined 12 weeks after start of treatment. *Own presentation S. Staudte, unpublished data.*

In my pilot study, the exploratory CTC threshold of ≥ 3 CTCs /7.5ml was used. Subsequently, with the release of the findings from the KEYNOTE–048 study [22], which demonstrated that a CPS ≥ 20 is indicative of a response to ICI in R/M HNSCC, I adjusted my approach. For my ICI CTC study, a cut–off for CTC positivity of ≥ 5 CTCs /7.5 ml was implemented. Due to this adjustment a statistical significance for PD–L1 positivity, ensuring that at least one out of five CTCs (20%) was PD–L1^{positive}, was established. These two cut–off values were used for subsequent analysis.

CTC positivity is more frequently expected in patients diagnosed with distant metastasis. However, analysis of my cohort did not reveal any correlation between CTC positivity and site of progression (Table 7, Figure 11). Of the locally recurrent patients 10/21 (47.6%) were tested CTC^{positive} and 8/33 (24.2%) of the patients with distant metastasis.

Table 7: Patients classified according to their CTC status and the site of progression.
Own presentation S. Staudte, unpublished data.

Site of progression	$CTC^{negative}$ (< 5 CTCs/ 7.5ml)	$CTC^{positive}$ (≥ 5 CTCs/ 7.5ml)	Total cases n (%)
Locally recurrent (incl. LN)	11 (52.4%)	10 (47.6%)	21 (100%)
Distant metastasis	25 (75.8%)	8 (24.2%)	33 (100%)
Total cases	36 (66.7%)	18 (33.3%)	54 (100%)

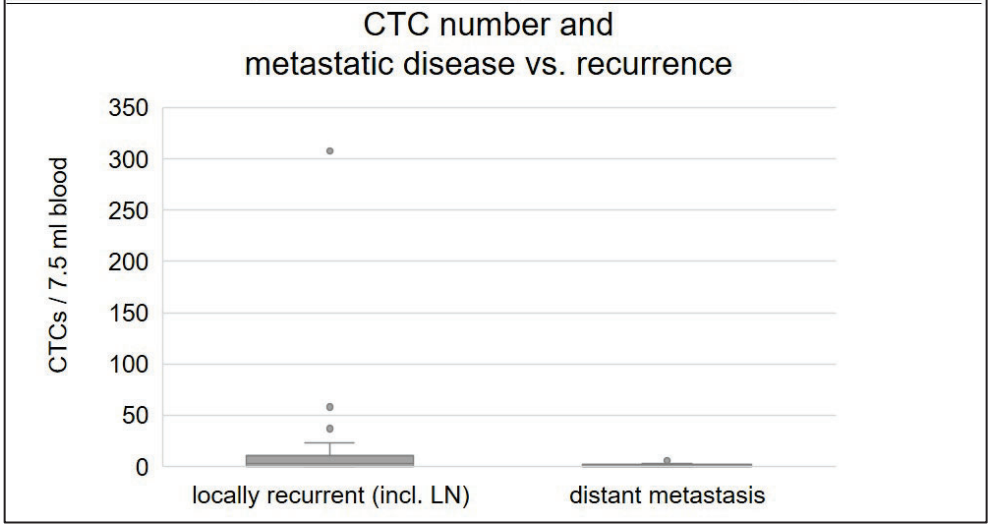

Figure 11: Number of CTCs clustered to the site of progression. Number of detected CTCs /7.5 ml blood collected at baseline from patients with R/M HNSCC. *Own presentation S. Staudte, unpublished data.*

Using the cut–off value of ≥ 5 CTCs /7.5 ml for CTC analysis at baseline, a CTC positivity rate of 33.3% (18/54) was observed. PFS and OS analysis independent on the PD–L1 status of CTCs and CPS revealed no significant correlation between CTC positivity and reduced PFS /OS (Figure 12A/B). The detailed analysis of $CTC^{positive}$ patients being tested either $PD–L1^{positive}$ (7/18; 38.9%) or $PD–L1^{negative}$ (11/18; 61.1%;

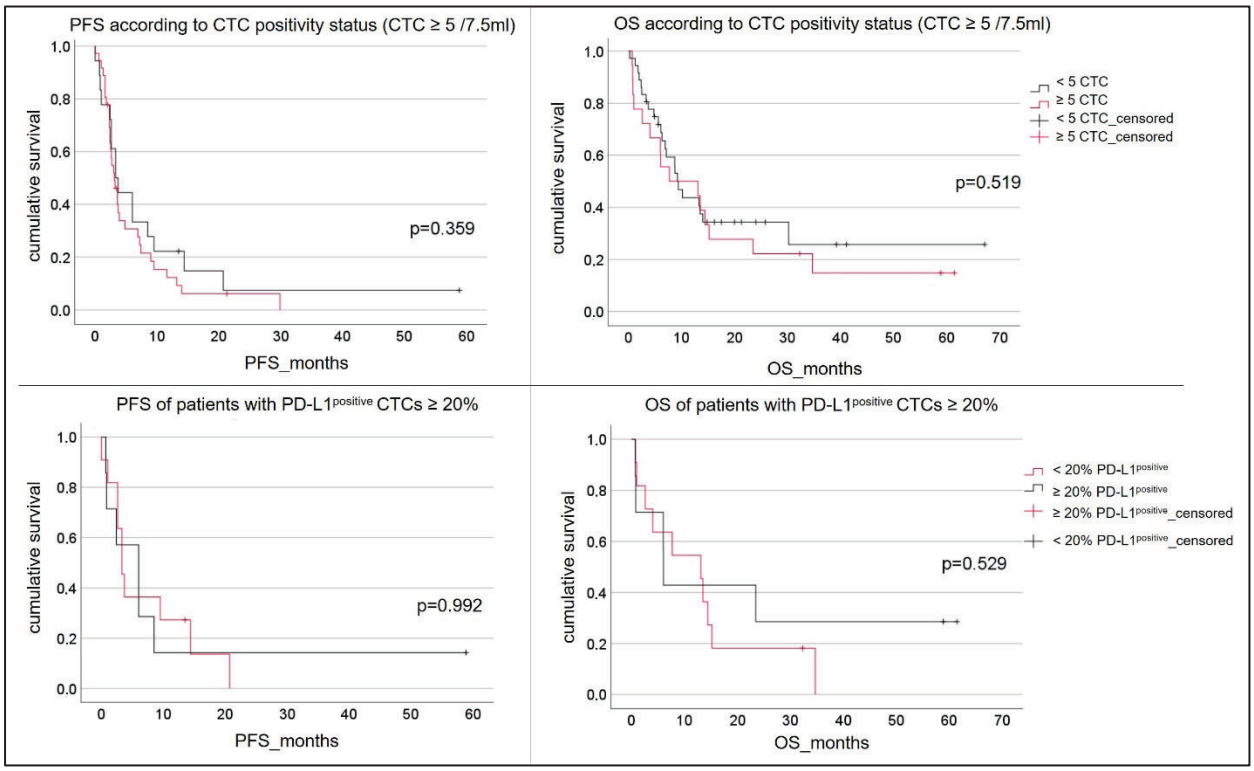

Figure **12** C/D) revealed also no significant influence on PFS or OS.

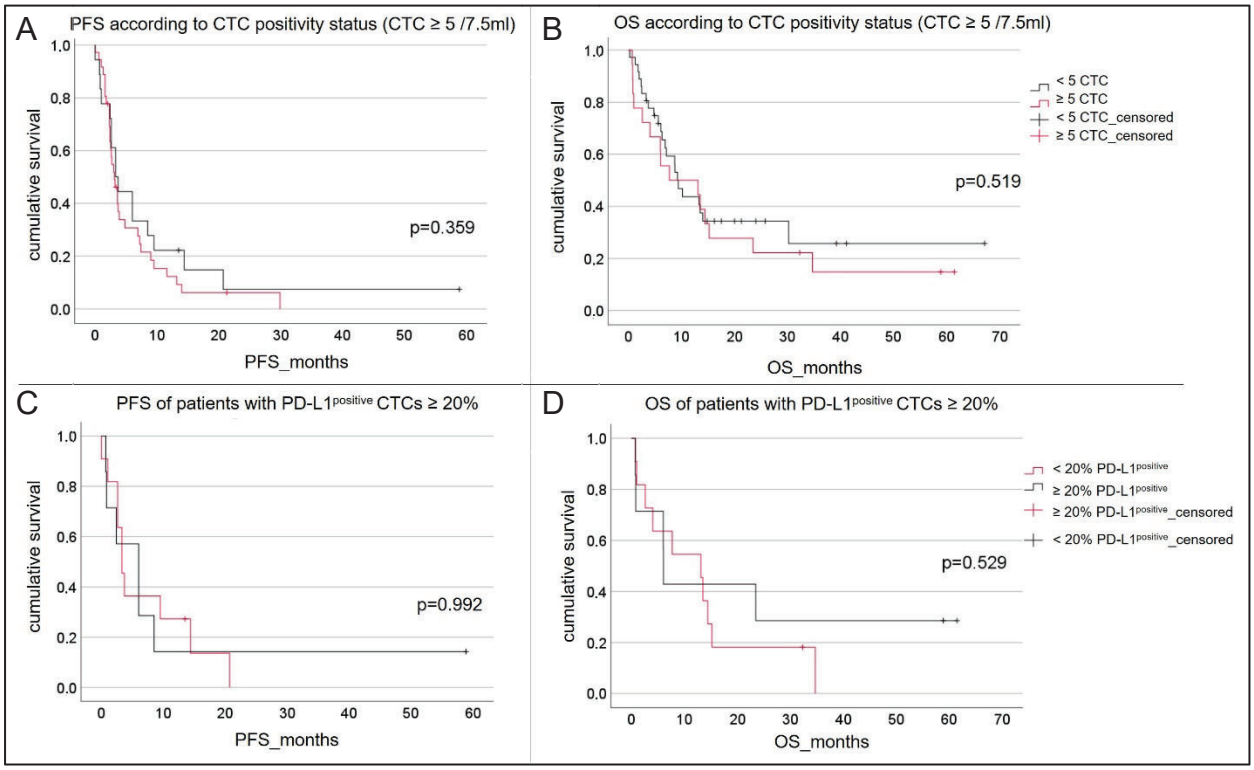

Figure 12: Analysis of PFS and OS according to the CTC status and PD–L1 expression. PD–L1 analysis was based on the data of patients tested CTC^{positive} at baseline. *Own presentation S. Staudte, unpublished data.*

In order to investigate the impact of PD–L1 expression on PFS in either tumour tissue (CPS ≥ 20) and /or in CTCs (≥ 20%), the patients were clustered according to their PD–L1 status in both specimen. Thus resulting in a cluster of patients being negative in both, positive in one or positive for both samples. Survival analysis based on these three groups revealed a significant better PFS of patients tested PD–L1^{positive} in both tissue and liquid biopsy compared to the other groups (Figure 13, purple line). In contrast to those data shown in Figure 12, it has to be emphasised, that the data shown in Figure 13 were based on patients a CPS was available.

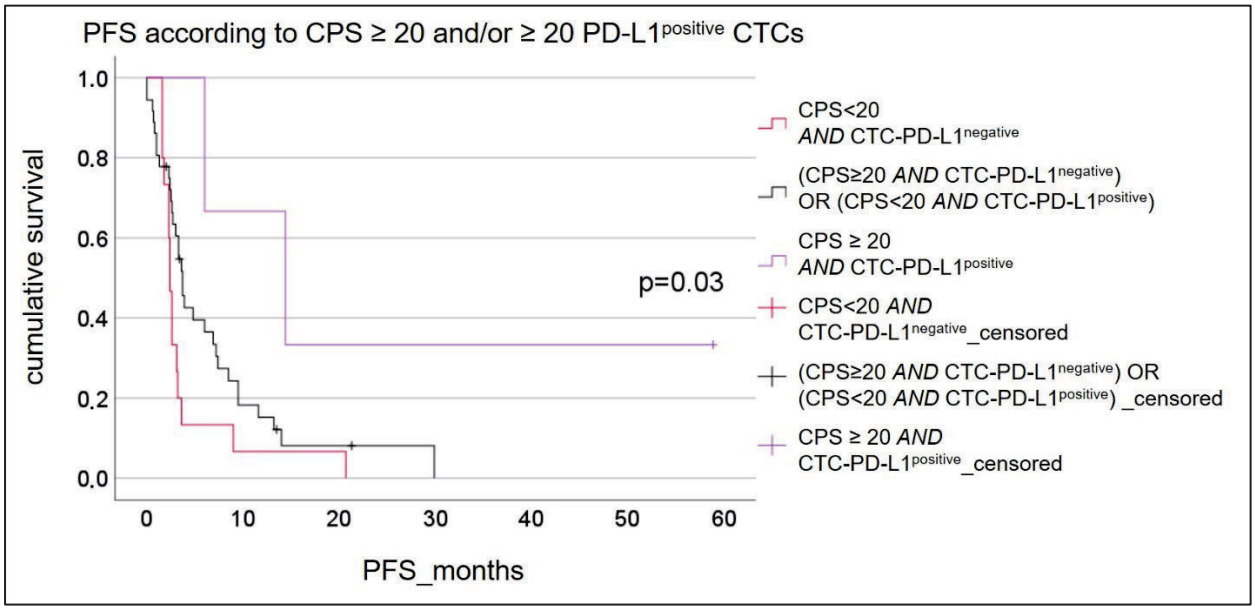

Figure 13: PFS analysis in correlation to the PD–L1 status in tumour and liquid biopsy. PFS analysis of ICI–treated patients based on PD–L1 positivity of tumour tissue and /or CTCs. Patients with CPS ≥ 20 or PD-L1 expression ≥ 20% on CTCs had a significant (p=0.03) better PFS compared to the other two groups. OS analysis did result in a significant correlation. *Own presentation S. Staudte, unpublished data.*

In order to investigate the clinical meaning of treatment–induced dynamical changes in CTC numbers, Kaplan–Meier survival analysis was performed. Separation of survival curves emphasizes that patients with a consistent CTC status had a better OS compared to those experiencing a change in CTC numbers (Figure 14 B). A more detailed analysis allowed a grouping of the patients into four distinct groups: patients with persisting CTCs (10/31), becoming CTC^{positive} under treatment (5/31), patients remaining CTC^{negative} (11/31) and becoming CTC^{negative} after 12 weeks of treatment (5/31). PFS and OS analysis of the subgroups did not result in a significant separation of the survival

curves, neither for those having a stable nor experiencing a change in CTC status (Figure 14 C–D). Stable CTC status over time of treatment was more frequent in the overall cohort.

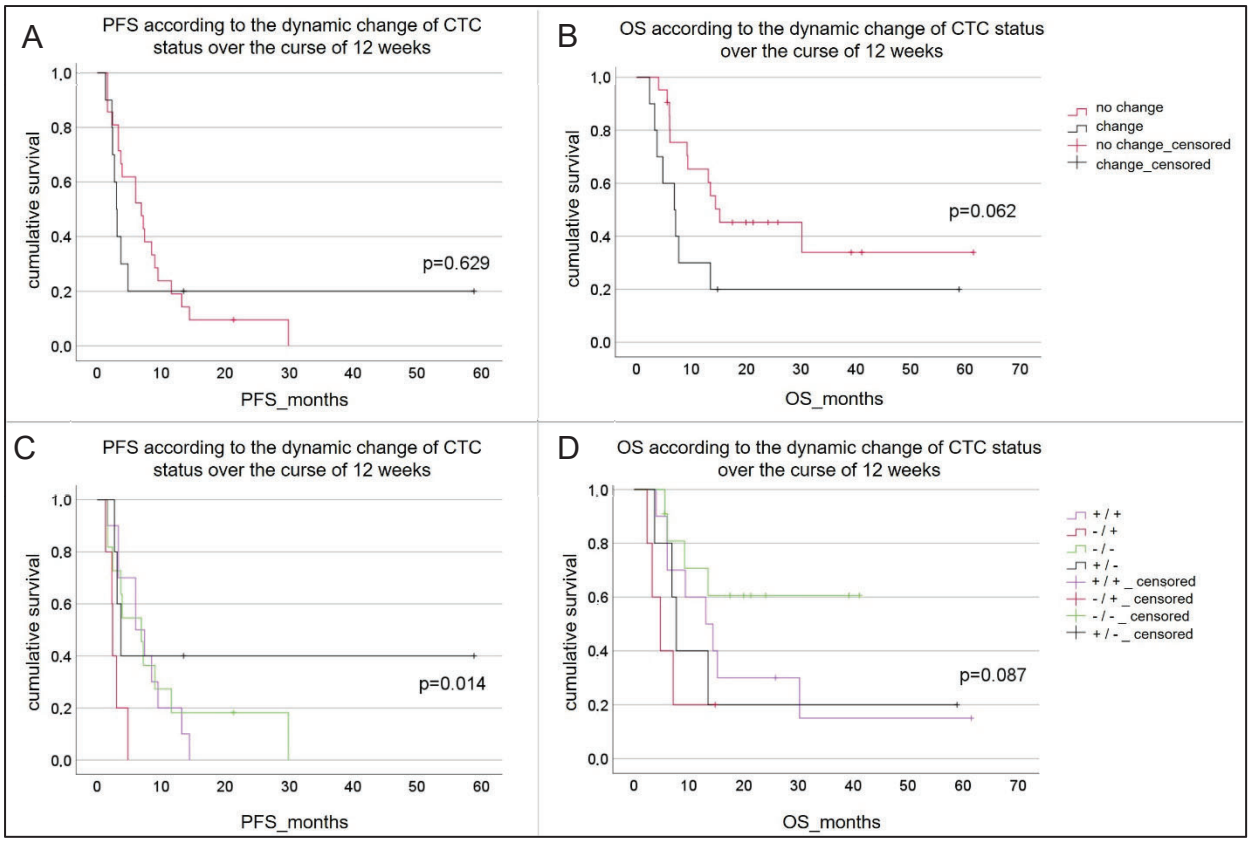

Figure 14: Survival analysis regarding the dynamic change of CTC counts during treatment. Analysis of changes in CTC status over time (T0–T2) and the impact on (A) PFS and (B) OS. (C–D) Four subgroups were classified: persisting CTCs (n=10; +/+), consistently negative for CTCs (n=11; -/-), patients becoming $CTC^{positive}$ (n=5; -/+) and those becoming $CTC^{negative}$ (n=5; +/-) during the course of treatment. In total blood samples of 31 patients have been used for kinetic analysis of CTC counts. Detailed analysis using Log-Rank test revealed a significant better PFS for (+/+) over (-/+)-patients (p=0.003), exclusively. *Own presentation S. Staudte, unpublished data.*

The amount of patients tested positive for PD–L1 expressing CTCs increases over the course of therapy, but the number of patients being available for blood collection for CTC analysis decreased due to disease related events. Thus, $PD–L1^{positive}$ CTCs were detected in 38.8% of patients (7/18) at baseline, 40% (6/15) at T1 and 60% (6/10) at T2. Kinetic analysis of the PD–L1 status over time (T0–T2) did not reveal any statistical significance.

4 Discussion

4 .1 Short summary of results

This is the first study demonstrating the suitability of the ISX for comprehensive phenotyping of CTCs in R/M HNSCC. In order to investigate the prognostic potential of CTCs, the focus was set to markers, representing the immune status of CTCs, the activation status of oncogenic signalling pathways and the response to DNA damage by radiotherapy. Thus, stainings for PD–L1 /–L2, phospho–EGFR and γH2AX foci were established, accordingly. EpCAM and EGFR were used as tumour cell selection markers, to detect CTCs of either epithelial or pEMT phenotypes. CD45 was used as a marker for leukocytes, which were excluded from subsequent analysis.

By performing spiking experiments, high sensitivity (73%) and specificity (100%) of my established ISX–based CTC assay were demonstrated. In the pilot study, suitability of my assay for CTC analysis in patient blood samples has been proven ($CTC^{positive}$ cases with a cut–off value of ≥ 3 CTCs /7.5ml blood: HNSCC 44% and BC 75%). The subsequent clinical observational study (ICI CTC trial) aimed at investigating the clinical value of PD–L1 expressing CTCs in R/M HNSCC. In 33% of the samples, successful CTC detection and analysis of their immune checkpoint status was achieved. However, no concordance of PD–L1 expression between tissue and liquid biopsy was observed in neither study. Since a cut–off value of CTC numbers for predicting 6–months survival could not be identified by ROC analysis in my study, an exploratory cut–off for CTC positivity was set to ≥ 5 CTCs /7.5ml and 20% (1 /5 CTCs) PD–L1 positivity and applied to the data of the ICI CTC trial. The patients were clustered into three groups based on their PD–L1 status in tissue and /or corresponding CTCs, accordingly. Kaplan–Meier analysis revealed a survival benefit for patients diagnosed with CPS ≥ 20 and ≥ 20% PD–L1 expressing CTCs, followed by those being tested $PD–L1^{positive}$ in either tissue or liquid biopsy. Analysis of CTC counts alone or in combination with their PD–L1 expression below the cut–offs in both tumour tissue (CPS < 20) and CTCs (<20%) showed decreased PFS compared to patients with higher PD–L1 expression, although this difference in outcome was not significant.

4.2 Interpretation of results

ICIs targeting PD–1 or its ligand PD–L1, have gained attention in the last decade and shown good response rates in various tumour entities [18, 20, 23]. Due to the limitation of tissue biopsy to capture the entire intra–tumour heterogeneity and the dynamic change of tumour marker expression under treatment pressure, I aimed at investigating the prognostic and predictive value of PD–L1^{positive} CTCs for patient stratification for ICI in R/M HNSCC. Thus, I established a protocol for CTC enrichment followed by ISX–based detection of CTCs and their PD–L1 /–L2 expression. My recovery rate of 73% was consistent with other ISX–based CTC studies who reported results between 44–73% [24-26]. The additional use of EGFR as a tumour marker, which is also expressed in HNSCC which underwent pEMT might capture a larger diversity of CTC phenotypes, yielding improved recovery rates of my assay [13]. This also results in a better representation of the tumour cell population in its overall heterogeneity by CTCs [27]. Especially when spiking low cell numbers (5 cells /4ml) I could demonstrate robust sensitivity, while López–Riquelme et al. had reduced sensitivity with decreasing cell numbers < 10 cells [28]. Although 1 out of 11 healthy donor samples has been tested CTC^{positive} (2 CTCs /7.5ml blood), with the cut–off value of ≥ 3 CTCs /7.5ml an assay specificity of 100% was achieved. The presence of EpCAM–EGFR positive cells in blood samples from healthy donors most likely resulted from a contamination by normal epithelial cells during blood draw procedure, since the first millilitre was not discarded. However, the presence of a tumour that has not yet been discovered cannot be ruled out [29].

CTC analysis of BC patient blood samples identified 75% of the patients (6/8) as CTC^{positive} (CTC numbers ranging from 9–17) of which 67% had PD-L1^{positive} CTCs. Detailed analysis of primary vs. metastatic cases revealed that 100% (4/4) mBC cases were tested CTC^{positive}; of which one had PD-L1^{positive} CTCs (≥ 20%). Comparing the data of mBC cases with the results from Darga et al. (mBC, n=124, 42% CTC^{positive}), my assay demonstrated significant better CTC detection frequency [30]. However, the low sample numbers analysed in my project does not allow a firm conclusion on potential differences in the sensitivity of the CTC detection assays. Their analysis was based on the FDA–approved CS. In order to compare the performance of both assays, a study analysing blood samples from the same patient on both devices in parallel, is required [28].

Investigating the diagnostic value of PD–L1 expressing CTCs in R/M HNSCC was the main research focus and consequently a larger study focusing on patients treated with

anti–PD–1 inhibitors was conducted. To my knowledge, only a few clinical studies have been conducted to investigate the prognostic and predictive value of both the CTC count and PD–L1 status of CTCs in R/M HNSCC. Kulasinghe et al. [31] and Tada et al.[32] have shown CTC detection frequencies of 47.8% (11/23) to 63.3% (28/44) in their cohorts composed of patients with disease stage I–IV, respectively. Both studies performed size–based CTC enrichment and cytokeratin staining for quantification. The former used IF staining for PD–L1 detection on CTCs (54.4% of $CTC^{positive}$ cases), whereas the others used RT–PCR (39.3% of $CTC^{positive}$ cases). Analysis of my data revealed a CTC positivity in 33.3% (18/54) of patients, of which 38.9% (7/18) were tested $PD–L1^{positive}$. Our reduced detection rate might be explained by the different enrichment and detection methods used as well as by the fact that the two groups did not define a cut–off for CTC positivity.

Interestingly, Zhou et al, showed that classification of patients according to baseline CTC PD–L1 expression intensity (low, medium, high) can identify patients with distinct clinical response to ICI–treatment [23]. Moreover, detection of PD–L1 overexpressing CTCs post–treatment, has been shown to be prognostic for reduced PFS [33]. Analysis of the PD–L1 status prior and post treatment in our cohort did not show any clinical significance, even though inter–patient heterogeneity in PD–L1 expression was observed. Due to the low case number, classification accordingly to the PD–L1 expression intensity was not meaningful, but might be useful for future studies with larger patient numbers.

Paired analysis of PD–L1 expression in tumour tissue and corresponding liquid biopsy was performed on cases with detectable CTCs and known CPS status. Analysis of our R/M HNSCC cohort revealed a concordant PD–L1 status in only 40% in these cases. Lacking concordance between PD–L1 status of tissue and corresponding liquid biopsy was frequently reported [3], while some have shown moderate concordance of 43.5% in R/M HNSCC [34] or 42.3% in NCSLC [35]. However, a concordance rate of 40% is not sufficient for implementation into clinical routine, although CTC measurement as well as analysis of their PD–L1 status can be a useful complement to the conventional tumour biopsy.

HNSCC exhibits frequent overexpression of EGFR, and activated EGFR signalling has been shown to induce PD–L1 expression [36]. Thus, staining of activated EGFR was implemented in my CTC assay. Activated EGFR signalling is involved in the regulation of the activity of DNA protein kinases, which are part of the DNA repair machinery [37], thereby potentially contributing to radioresistance. In addition, it was shown that irradiation itself induces the release of vital tumour cells into blood circulation, being

potential precursors for distant metastasis [38], which is an important aspect considering that radiotherapy is the standard of care for L/A HNSCC [39].
Thus, by the inclusion of phospho–EGFR analysis and quantification of the response marker to radiotherapy (γH2AX), my CTC assay may provide a suitable tool for real–time monitoring of a) changes in CTCs numbers due to radiotherapy and b) response to radiotherapy and ICI by quantifying γH2AX foci and PD–L1^{positive} CTCs, respectively. Application of this assay for comprehensive profiling of CTCs is planned in a future clinical trial.

4.3 Embedding the results into the current state of research

To my knowledge, only a few studies (n=10) have evaluated the applicability of the ISX system for CTC detection and more detailed phenotyping. With my work, I have provided additional data, supporting the usability of the ISX for CTC analyses, especially with the focus on CTC detection in R/M HNSCC.
Curtin et al. intensively discussed the current state of research on CTCs in HNSCC [40]. While screening the literature they noticed that CTC studies in HNSCC predominantly include all subtypes of HNSCC, thus making the investigation of the prognostic /predictive value of CTCs in HNSCC difficult. It has been hypothesized that depending on the tumours origin, the diagnostic potential of CTCs might vary.
There is evidence that the combination of various marker improved CTC detection [41]. The use of different methods also makes it difficult to compare the results of individual CTC studies in HNSCC. Most frequently, CTCs in HNSCC were shown to be predictive for disease progression [31]. Our results neither confirm nor disprove these statements.
PD–L1 is approved as a tissue biomarker to predict response to ICI therapy. However, there is still a significant amount of patients not responding to ICI although tested PD–L1^{positive} and vice versa [4] which might be due the dynamic expression of PD–L1 during treatment [42]. Thus, research is ongoing to investigate the predictive value of PD–L1^{positive} CTCs, by performing serial sampling during treatment. According to the results of Kulasinghe at el. PD–L1^{positive} CTCs in HNSCC (n=23) are not predictive for therapy response [31]. Strati et al. found that at baseline PD–L1^{positive} CTCs are not prognostic for HNSCC (n=113). However, they performed serial sampling and revealed that persistent PD–L1^{positive} CTCs were associated with reduced PFS. [33], which was also observed by Nicolazzo et al.in mNSCLC (n=24) [4]. My data do not indicate that CTC numbers or their

PD–L1 positivity have any predictive or prognostic value for R/M HNSCC. However, I could demonstrate that by combining the CPS and the PD–L1 status of the detected CTCs, patients with improved benefit from ICI treatment could be identified. This may indicate that a combination of both markers could help to improve patient stratification for ICI treatment.

4.4 Strengths and weaknesses of the study

One of the major strengths of this novel assay for CTC detection in HNSCC is the combined use of EpCAM and EGFR as tumour detection markers. Due to this combination, it is feasible to capture both epithelial–like CTCs and those under pEMT, thereby increasing the possibility to capture a larger amount of CTC subclones throughout their heterogeneous phenotypes. This is of special interest, because CTCs with an EMT /pEMT phenotype were shown to have a higher metastatic potential compared to epithelial–like CTCs and thus may represent the clinically more relevant CTC subpopulation. Further, the flexibility of my ISX–based CTC assay to be adapted to different tumour entities and markers of interest makes it a powerful tool for comprehensive phenotyping of CTCs.

Interpreting the performance of the ISX–CTC assay would require a direct comparison with the FDA–approved CS. López–Riquelme et al. have already performed a head–to–head comparison of both devices, showing comparable performance, when using EpCAM as tumour cell marker [28].

The composition of the used patient cohort limits the statistical power of this study. The majority of the enrolled patients was male (83.3%) with a median age of 70 years. Further, most of them had a reduced performance status at time of recruitment. When coupled with the advanced stage of the disease, this factor might have influenced the treatment outcome, irrespective of CTC count and PD–L1 expression. The focus of my study on R/M HNSCC was based on the expectation to detect a higher number of CTCs, compared to patients at early stages. Yet, given the limited total number of patients enrolled in the study and the fact that only 33.3% of cases tested $CTC^{positive}$, the study lacked the statistical power needed to establish a prognostic CTC cut–off value for positivity. Further, no association between PD–L1 status of CTCs and clinical outcome was observed which is contradictory to data from other working group. No correlation was seen between site of progression and the presence of CTCs. Further investigation of the diagnostic value of

CTCs in R/M HNSCC treated with ICI alone and in combination with radiotherapy in a subsequent study is warranted.

4.5 Implications for practice and/or future research

It is planned to apply the extended ISX–CTC assay to a more heterogeneous patient cohort of HNSCC, including all stages and treatment strategies available in order to identify whether the prognostic and predictive value of CTCs for all HNSCC patients can be improved. Establishment of the diagnostic value of CTCs for patients with early disease and for those who develop rapid resistance is of special need and interest. In particular, the combination of PD–L1, phospho–EGFR and γH2AX foci hold promising potential to be used as a CTC biomarker, because thereby the response to combined treatment can be determined by a single liquid biopsy.

Further, these three markers are connected with each other through various signalling cascades. Radiation was shown to induce ligand–independent activation of EGFR, by which downstream pathways are activated. One of them regulates the activity of a key enzyme of the DNA repair machinery, promoting resistance to radiotherapy. It has also been shown that irradiation and as a consequence EGFR signalling have a modulating effect on the immune system and can therefore also induce PD–L1 expression, resulting in surface and intra–nuclear PD–L1 expression. The latter one has been associated with resistance to radiotherapy.

Radiotherapy is still the standard of care for LA HNSCC, it was recently shown, that neoadjuvant treatment with Pembrolizumab improves the overall clinical outcome of treatment naïve patients, compared to standard of care [43]. Although the preliminary results are promising, there were still patients not having a benefit from this neoadjuvant treatment. This emphasises that a tissue biopsy might not capture the entire heterogeneity, resulting in an underestimation of potentially therapy resistant subclones. Thus, subsequent CTC analysis for real–time monitoring of therapy response might help to adjust treatment in an early stage and thereby eventually prevent rapid progress.

5 Conclusions

I have established a novel method for comprehensive phenotyping of CTCs in HNSCC. Flexibility of my assay to be used for different tumour entities could be demonstrated by additionally analysing breast cancer samples. Due to the combination of EpCAM and EGFR as tumour markers, my assay achieved better recovery frequencies, compared to the data of other groups using EpCAM only. Finally, its suitability has been demonstrated in a larger clinical trial composed of R/M HNSCC patients who received treatment with ICI. Although I could not establish a predictive and /or prognostic value of PD–L1 expressing CTCs in R/M HNSCC, I was able to generate promising preliminary data, which have to be evaluated in a larger cohort. Based on my data, the combined analysis of baseline CPS and CTC PD–L1 status could be employed to identify and enrich for patients who are likely to respond to ICI. However, this hypothesis has to be investigated in another clinical trial. The ability to monitor therapy response stands out as a key feature of blood–based tumour markers, enabling adjustments in treatment strategies that can ultimately enhance patient outcomes. This potential is evident in my developed ISX–based CTC assay, which could be employed in subsequent clinical trials to explore the viability of CTCs as a biomarker for HNSCC.

Reference list

1. Herrscher, H. and C. Robert, *Immune checkpoint inhibitors in melanoma in the metastatic, neoadjuvant, and adjuvant setting.* Current Opinion in Oncology, 2020. **32**(2).
2. Zhu, P., Y. Wang, W. Zhang, and X. Liu, *Anti-PD1/PD-L1 monotherapy vs standard of care in patients with recurrent or metastatic head and neck squamous cell carcinoma: A meta-analysis of randomized controlled trials.* Medicine, 2021. **100**(4): p. e24339-e24339.
3. Strati, A., P. Economopoulou, E. Lianidou, and A. Psyrri, *Clinical Significance of PD-L1 Status in Circulating Tumor Cells for Cancer Management during Immunotherapy.* Biomedicines, 2023. **11**(6): p. 1768.
4. Nicolazzo, C., C. Raimondi, M. Mancini, S. Caponnetto, A. Gradilone, O. Gandini, M. Mastromartino, G. del Bene, A. Prete, F. Longo, E. Cortesi, and P. Gazzaniga, *Monitoring PD-L1 positive circulating tumor cells in non-small cell lung cancer patients treated with the PD-1 inhibitor Nivolumab.* Scientific Reports, 2016. **6**(1): p. 31726.
5. Pantel, K. and C. Alix-Panabières, *Crucial roles of circulating tumor cells in the metastatic cascade and tumor immune escape: biology and clinical translation.* J Immunother Cancer, 2022. **10**(12).
6. Jie, X.-X., X.-Y. Zhang, and C.-J. Xu, *Epithelial-to-mesenchymal transition, circulating tumor cells and cancer metastasis: Mechanisms and clinical applications.* Oncotarget, 2017. **8**(46): p. 81558-81571.
7. Diamantopoulou, Z., F. Castro-Giner, F.D. Schwab, C. Foerster, M. Saini, S. Budinjas, K. Strittmatter, I. Krol, B. Seifert, V. Heinzelmann-Schwarz, C. Kurzeder, C. Rochlitz, M. Vetter, W.P. Weber, and N. Aceto, *The metastatic spread of breast cancer accelerates during sleep.* Nature, 2022. **607**(7917): p. 156-162.
8. Tellez-Gabriel, M., M.-F. Heymann, and D. Heymann, *Circulating Tumor Cells as a Tool for Assessing Tumor Heterogeneity.* Theranostics, 2019. **9**(16): p. 4580-4594.
9. Cristofanilli, M., G.T. Budd, M.J. Ellis, A. Stopeck, J. Matera, M.C. Miller, J.M. Reuben, G.V. Doyle, W.J. Allard, L.W. Terstappen, and D.F. Hayes, *Circulating tumor cells, disease progression, and survival in metastatic breast cancer.* N Engl J Med, 2004. **351**(8): p. 781-91.
10. Cohen, S.J., C.J.A. Punt, N. Iannotti, B.H. Saidman, K.D. Sabbath, N.Y. Gabrail, J. Picus, M.A. Morse, E. Mitchell, M.C. Miller, G.V. Doyle, H. Tissing, L.W.M.M. Terstappen, and N.J. Meropol, *Prognostic significance of circulating tumor cells in patients with metastatic colorectal cancer.* Annals of Oncology, 2009. **20**(7): p. 1223-1229.
11. Vidlarova, M., A. Rehulkova, P. Stejskal, A. Prokopova, H. Slavik, M. Hajduch, and J. Srovnal, *Recent Advances in Methods for Circulating Tumor Cell Detection.* International Journal of Molecular Sciences, 2023. **24**(4): p. 3902.
12. Staudte, S., K. Klinghammer, P.S. Jurmeister, P. Jank, J.-U. Blohmer, S. Liebs, P. Rhein, A.E. Hauser, and I. Tinhofer, *Multiparametric Phenotyping of Circulating Tumor Cells for Analysis of Therapeutic Targets, Oncogenic Signaling Pathways and DNA Repair Markers.* Cancers, 2022. **14**(11): p. 2810.
13. Holz, C., F. Niehr, M. Boyko, T. Hristozova, L. Distel, V. Budach, and I. Tinhofer, *Epithelial-mesenchymal-transition induced by EGFR activation interferes with cell migration and response to irradiation and cetuximab in head and neck cancer cells.* Radiother Oncol, 2011. **101**(1): p. 158-64.

14. Durdik, M., P. Kosik, J. Gursky, L. Vokalova, E. Markova, and I. Belyaev, *Imaging flow cytometry as a sensitive tool to detect low-dose-induced DNA damage by analyzing 53BP1 and γH2AX foci in human lymphocytes.* Cytometry Part A, 2015. **87**(12): p. 1070-1078.
15. Liu, Z., A. Fusi, E. Klopocki, A. Schmittel, I. Tinhofer, A. Nonnenmacher, and U. Keilholz, *Negative enrichment by immunomagnetic nanobeads for unbiased characterization of circulating tumor cells from peripheral blood of cancer patients.* J Transl Med, 2011. **9**: p. 70.
16. Brown, T.C., N.V. Sankpal, and W.E. Gillanders, *Functional Implications of the Dynamic Regulation of EpCAM during Epithelial-to-Mesenchymal Transition.* Biomolecules, 2021. **11**(7): p. 956.
17. Keller, L., S. Werner, and K. Pantel, *Biology and clinical relevance of EpCAM.* Cell Stress, 2019. **3**(6): p. 165-180.
18. Wang, Y., T.H. Kim, S. Fouladdel, Z. Zhang, P. Soni, A. Qin, L. Zhao, E. Azizi, T.S. Lawrence, N. Ramnath, K.C. Cuneo, and S. Nagrath, *PD-L1 Expression in Circulating Tumor Cells Increases during Radio(chemo)therapy and Indicates Poor Prognosis in Non-small Cell Lung Cancer.* Scientific Reports, 2019. **9**(1): p. 566.
19. Cohen, E.E.W., R.B. Bell, C.B. Bifulco, B. Burtness, M.L. Gillison, K.J. Harrington, Q.T. Le, N.Y. Lee, R. Leidner, R.L. Lewis, L. Licitra, H. Mehanna, L.K. Mell, A. Raben, A.G. Sikora, R. Uppaluri, F. Whitworth, D.P. Zandberg, and R.L. Ferris, *The Society for Immunotherapy of Cancer consensus statement on immunotherapy for the treatment of squamous cell carcinoma of the head and neck (HNSCC).* J Immunother Cancer, 2019. **7**(1): p. 184.
20. Ferris, R.L., G. Blumenschein, Jr., J. Fayette, J. Guigay, A.D. Colevas, L. Licitra, K. Harrington, S. Kasper, E.E. Vokes, C. Even, F. Worden, N.F. Saba, L.C. Iglesias Docampo, R. Haddad, T. Rordorf, N. Kiyota, M. Tahara, M. Monga, M. Lynch, W.J. Geese, J. Kopit, J.W. Shaw, and M.L. Gillison, *Nivolumab for Recurrent Squamous-Cell Carcinoma of the Head and Neck.* N Engl J Med, 2016. **375**(19): p. 1856-1867.
21. Seiwert, T.Y., B. Burtness, R. Mehra, J. Weiss, R. Berger, J.P. Eder, K. Heath, T. McClanahan, J. Lunceford, C. Gause, J.D. Cheng, and L.Q. Chow, *Safety and clinical activity of pembrolizumab for treatment of recurrent or metastatic squamous cell carcinoma of the head and neck (KEYNOTE-012): an open-label, multicentre, phase 1b trial.* The Lancet Oncology, 2016. **17**(7): p. 956-965.
22. Burtness, B., K.J. Harrington, R. Greil, D. Soulières, M. Tahara, G. de Castro, A. Psyrri, N. Basté, P. Neupane, Å. Bratland, T. Fuereder, B.G.M. Hughes, R. Mesía, N. Ngamphaiboon, T. Rordorf, W.Z. Wan Ishak, R.-L. Hong, R. González Mendoza, A. Roy, Y. Zhang, B. Gumuscu, J.D. Cheng, F. Jin, D. Rischin, G. Lerzo, M. Tatangelo, M. Varela, J.J. Zarba, M. Boyer, H. Gan, B. Gao, B. Hughes, G. Mallesara, D. Rischin, A. Taylor, M. Burian, T. Fuereder, R. Greil, C.H. Barrios, D.O. de Castro Junior, G. Castro, F.A. Franke, G. Girotto, I.P.F. Lima, U.R. Nicolau, G.D.J. Pinto, L. Santos, A.-P. Victorino, N. Chua, F. Couture, R. Gregg, A. Hansen, J. Hilton, J. McCarthy, D. Soulieres, R. Ascui, P. Gonzalez, L. Villanueva, M. Torregroza, A. Zambrano, P. Holeckova, Z. Kral, B. Melichar, J. Prausova, M. Vosmik, M. Andersen, N. Gyldenkerne, H. Jurgens, K. Putnik, P. Reinikainen, V. Gruenwald, S. Laban, G. Aravantinos, I. Boukovinas, V. Georgoulias, A. Psyrri, D. Kwong, Y. Al-Farhat, T. Csoszi, J. Erfan, G. Horvai, L. Landherr, E. Remenar, A. Ruzsa, J. Szota, S. Billan, I. Gluck, O. Gutfeld, A. Popovtzer, M. Benasso, S. Bui, V. Ferrari, L. Licitra, F. Nole, T. Fujii, Y. Fujimoto,

N. Hanai, H. Hara, K. Matsumoto, K. Mitsugi, N. Monden, M. Nakayama, K. Okami, N. Oridate, K. Shiga, Y. Shimizu, M. Sugasawa, M. Tahara, M. Takahashi, S. Takahashi, K. Tanaka, T. Ueda, H. Yamaguchi, T. Yamazaki, R. Yasumatsu, T. Yokota, T. Yoshizaki, I. Kudaba, Z. Stara, W.Z. Wan Ishak, S.K. Cheah, J. Aguilar Ponce, R. Gonzalez Mendoza, C. Hernandez Hernandez, F. Medina Soto, J. Buter, A. Hoeben, S. Oosting, K. Suijkerbuijk, A. Bratland, M. Brydoey, R. Alvarez, L. Mas, P. Caguioa, J. Querol, E.E. Regala, M.B. Tamayo, E.M. Villegas, A. Kawecki, A. Karpenko, A. Klochikhin, A. Smolin, O. Zarubenkov, B.C. Goh, G. Cohen, J. du Toit, C. Jordaan, G. Landers, P. Ruff, W. Szpak, N. Tabane, I. Brana, L. Iglesias Docampo, J. Lavernia, R. Mesia, E. Abel, V. Muratidu, N. Nielsen, V. Cristina, T. Rordorf, S. Rothschild, R.-L. Hong, H.-M. Wang, M.-H. Yang, S.-P. Yeh, C.-J. Yen, N. Ngamphaiboon, N. Soparattanapaisarn, V. Sriuranpong, S. Aksoy, I. Cicin, M. Ekenel, H. Harputluoglu, O. Ozyilkan, K. Harrington, S. Agarwala, H. Ali, R. Alter, D. Anderson, J. Bruce, B. Burtness, N. Campbell, M. Conde, J. Deeken, W. Edenfield, L. Feldman, E. Gaughan, B. Goueli, B. Halmos, U. Hegde, B. Hunis, R. Jotte, A. Karnad, S. Khan, N. Laudi, D. Laux, D. Martincic, S. McCune, D. McGaughey, K. Misiukiewicz, D. Mulford, E. Nadler, P. Neupane, J. Nunnink, J. Ohr, M. O'Malley, B. Patson, D. Paul, E. Popa, S. Powell, R. Redman, V. Rella, C. Rocha Lima, A. Sivapiragasam, Y. Su, A. Sukari, S. Wong, E. Yilmaz and J. Yorio, *Pembrolizumab alone or with chemotherapy versus cetuximab with chemotherapy for recurrent or metastatic squamous cell carcinoma of the head and neck (KEYNOTE-048): a randomised, open-label, phase 3 study.* The Lancet, 2019. **394**(10212): p. 1915-1928.

23. Zhou, Y., J. Zhou, X. Hao, H. Shi, X. Li, A. Wang, Z. Hu, Y. Yang, Z. Jiang, and T. Wang, *Efficacy relevance of PD-L1 expression on circulating tumor cells in metastatic breast cancer patients treated with anti-PD-1 immunotherapy.* Breast Cancer Research and Treatment, 2023. **200**(2): p. 281-291.
24. Ruiz-Rodriguez, A.J., M.P. Molina-Vallejo, I. Aznar-Peralta, C. Gonzalez Puga, I. Canas Garcia, E. Gonzalez, J.A. Lorente, M.J. Serrano, and M.C. Garrido-Navas, *Deep Phenotypic Characterisation of CTCs by Combination of Microfluidic Isolation (IsoFlux) and Imaging Flow Cytometry (ImageStream).* Cancers (Basel), 2021. **13**(24).
25. Dent, B.M., L.F. Ogle, R.L. O'Donnell, N. Hayes, U. Malik, N.J. Curtin, A.V. Boddy, E.R. Plummer, R.J. Edmondson, H.L. Reeves, F.E. May, and D. Jamieson, *High-resolution imaging for the detection and characterisation of circulating tumour cells from patients with oesophageal, hepatocellular, thyroid and ovarian cancers.* Int J Cancer, 2016. **138**(1): p. 206-16.
26. Chudasama, D.Y., P. Katopodis, N. Stone, J. Haskell, H. Sheridan, B. Gardner, H.B. Urnovitz, E. Schuetz, J. Beck, M. Hall, J.G. Barr, C. Sisu, A.J. Rice, A. Polychronis, V. Anikin, and E. Karteris, *Liquid Biopsies in Lung Cancer: Four Emerging Technologies and Potential Clinical Applications.* Cancers, 2019. **11**.
27. Cohen, E.N., G. Jayachandran, H. Gao, P. Peabody, H.B. McBride, F.D. Alvarez, M. Kai, J. Song, Y. Shen, J.S. Willey, B. Lim, V. Valero, N.T. Ueno, and J.M. Reuben, *Phenotypic Plasticity in Circulating Tumor Cells Is Associated with Poor Response to Therapy in Metastatic Breast Cancer Patients.* Cancers, 2023. **15**(5): p. 1616.
28. Lopez-Riquelme, N., A. Minguela, F. Villar-Permuy, D. Ciprian, A. Castillejo, M.R. Alvarez-Lopez, and J.L. Soto, *Imaging cytometry for counting circulating tumor cells: comparative analysis of the CellSearch vs ImageStream systems.* APMIS, 2013. **121**(12): p. 1139-43.

29. Ried, K., P. Eng, and A. Sali, *Screening for Circulating Tumour Cells Allows Early Detection of Cancer and Monitoring of Treatment Effectiveness: An Observational Study.* Asian Pac J Cancer Prev, 2017. **18**(8): p. 2275-2285.
30. Darga, E.P., E.M. Dolce, F. Fang, K.M. Kidwell, C.L. Gersch, S. Kregel, D.G. Thomas, A. Gill, M.E. Brown, S. Gross, M. Connelly, M. Holinstat, E.F. Cobain, J.M. Rae, D.F. Hayes, and C. Paoletti, *PD-L1 expression on circulating tumor cells and platelets in patients with metastatic breast cancer.* PLoS One, 2021. **16**(11): p. e0260124.
31. Kulasinghe, A., J. Kapeleris, R. Kimberley, S.R. Mattarollo, E.W. Thompson, J.P. Thiery, L. Kenny, K. O'Byrne, and C. Punyadeera, *The prognostic significance of circulating tumor cells in head and neck and non-small-cell lung cancer.* Cancer Med, 2018. **7**(12): p. 5910-5919.
32. Tada, H., H. Takahashi, Y. Kuwabara-Yokobori, M. Shino, and K. Chikamatsu, *Molecular profiling of circulating tumor cells predicts clinical outcome in head and neck squamous cell carcinoma.* Oral Oncology, 2020. **102**: p. 104558.
33. Strati, A., G. Koutsodontis, G. Papaxoinis, I. Angelidis, M. Zavridou, P. Economopoulou, I. Kotsantis, M. Avgeris, M. Mazel, C. Perisanidis, C. Sasaki, C. Alix-Panabières, E. Lianidou, and A. Psyrri, *Prognostic significance of PD-L1 expression on circulating tumor cells in patients with head and neck squamous cell carcinoma.* Annals of Oncology, 2017. **28**(8): p. 1923-1933.
34. Chikamatsu, K., H. Tada, H. Takahashi, Y. Kuwabara-Yokobori, H. Ishii, S. Ida, and M. Shino, *Expression of immune-regulatory molecules in circulating tumor cells derived from patients with head and neck squamous cell carcinoma.* Oral Oncology, 2019. **89**: p. 34-39.
35. Guibert, N., M. Delaunay, A. Lusque, N. Boubekeur, I. Rouquette, E. Clermont, J. Mourlanette, S. Gouin, I. Dormoy, G. Favre, J. Mazieres, and A. Pradines, *PD-L1 expression in circulating tumor cells of advanced non-small cell lung cancer patients treated with nivolumab.* Lung Cancer, 2018. **120**: p. 108-112.
36. Akbay, E.A., S. Koyama, J. Carretero, A. Altabef, J.H. Tchaicha, C.L. Christensen, O.R. Mikse, A.D. Cherniack, E.M. Beauchamp, T.J. Pugh, M.D. Wilkerson, P.E. Fecci, M. Butaney, J.B. Reibel, M. Soucheray, T.J. Cohoon, P.A. Janne, M. Meyerson, D.N. Hayes, G.I. Shapiro, T. Shimamura, L.M. Sholl, S.J. Rodig, G.J. Freeman, P.S. Hammerman, G. Dranoff, and K.K. Wong, *Activation of the PD-1 pathway contributes to immune escape in EGFR-driven lung tumors.* Cancer Discov, 2013. **3**(12): p. 1355-63.
37. Rodemann, H.P., K. Dittmann, and M. Toulany, *Radiation-induced EGFR-signaling and control of DNA-damage repair.* International Journal of Radiation Biology, 2007. **83**(11-12): p. 781-791.
38. Martin, O.A., R.L. Anderson, P.A. Russell, R.A. Cox, A. Ivashkevich, A. Swierczak, J.P. Doherty, D.H. Jacobs, J. Smith, S. Siva, P.E. Daly, D.L. Ball, R.F. Martin, and M.P. MacManus, *Mobilization of viable tumor cells into the circulation during radiation therapy.* Int J Radiat Oncol Biol Phys, 2014. **88**(2): p. 395-403.
39. Carvalho, A.L., M.K. Ikeda, J. Magrin, and L.P. Kowalski, *Trends of oral and oropharyngeal cancer survival over five decades in 3267 patients treated in a single institution.* Oral Oncology, 2004. **40**(1): p. 71-76.
40. Curtin, J., S.W. Choi, P.J. Thomson, and A.K.y. Lam, *Characterization and clinicopathological significance of circulating tumour cells in patients with oral squamous cell carcinoma.* International Journal of Oral and Maxillofacial Surgery, 2022. **51**(3): p. 289-299.

41. Balasubramanian, P., J.C. Lang, K.R. Jatana, B. Miller, E. Ozer, M. Old, D.E. Schuller, A. Agrawal, T.N. Teknos, T.A. Summers, Jr., M.B. Lustberg, M. Zborowski, and J.J. Chalmers, *Multiparameter analysis, including EMT markers, on negatively enriched blood samples from patients with squamous cell carcinoma of the head and neck.* PLoS One, 2012. **7**(7): p. e42048.
42. Patel, S.P. and R. Kurzrock, *PD-L1 Expression as a Predictive Biomarker in Cancer Immunotherapy.* Molecular Cancer Therapeutics, 2015. **14**(4): p. 847-856.
43. Uppaluri, R., K.M. Campbell, A.M. Egloff, P. Zolkind, Z.L. Skidmore, B. Nussenbaum, R.C. Paniello, J.T. Rich, R. Jackson, P. Pipkorn, L.S. Michel, J. Ley, P. Oppelt, G.P. Dunn, E.K. Barnell, N.C. Spies, T. Lin, T. Li, D.T. Mulder, Y. Hanna, I. Cirlan, T.J. Pugh, T. Mudianto, R. Riley, L. Zhou, V.Y. Jo, M.D. Stachler, G.J. Hanna, J. Kass, R. Haddad, J.D. Schoenfeld, E. Gjini, A. Lako, W. Thorstad, H.A. Gay, M. Daly, S.J. Rodig, I.S. Hagemann, D. Kallogjeri, J.F. Piccirillo, R.D. Chernock, M. Griffith, O.L. Griffith, and D.R. Adkins, *Neoadjuvant and Adjuvant Pembrolizumab in Resectable Locally Advanced, Human Papillomavirus–Unrelated Head and Neck Cancer: A Multicenter, Phase II Trial.* Clinical Cancer Research, 2020. **26**(19): p. 5140-5152.

Statutory Declaration

“I, Stephanie Staudte, by personally signing this document in lieu of an oath, hereby affirm that I prepared the submitted dissertation on the topic [“Comprehensive profiling of circulating tumour cells for development of liquid biopsy biomarkers” /”Umfassende Charakterisierung von zirkulierenden Tumorzellen für die Biomarkerentwicklung aus der Flüssigbiopsie”], independently and without the support of third parties, and that I used no other sources and aids than those stated.
All parts which are based on the publications or presentations of other authors, either in letter or in spirit, are specified as such in accordance with the citing guidelines. The sections on methodology (in particular regarding practical work, laboratory regulations, statistical processing) and results (in particular regarding figures, charts and tables) are exclusively my responsibility.

Furthermore, I declare that I have correctly marked all of the data, the analyses, and the conclusions generated from data obtained in collaboration with other persons, and that I have correctly marked my own contribution and the contributions of other persons (cf. declaration of contribution). I have correctly marked all texts or parts of texts that were generated in collaboration with other persons.

My contributions to any publications to this dissertation correspond to those stated in the below joint declaration made together with the supervisor. All publications created within the scope of the dissertation comply with the guidelines of the ICMJE (International Committee of Medical Journal Editors; http://www.icmje.org) on authorship. In addition, I declare that I shall comply with the regulations of Charité – Universitätsmedizin Berlin on ensuring good scientific practice.

I declare that I have not yet submitted this dissertation in identical or similar form to another Faculty.

The significance of this statutory declaration and the consequences of a false statutory declaration under criminal law (Sections 156, 161 of the German Criminal Code) are known to me.”

Date Signature

Declaration of your own contribution to the publications

Stephanie Staudte contributed the following to the below listed publications:

Publication 1:

Staudte, S.; Klinghammer, K.; Jurmeister, P.S.; Jank, P.; Blohmer, J.-U.; Liebs, S.; Rhein, P.; Hauser, A.E.; Tinhofer, I. Multiparametric Phenotyping of Circulating Tumour Cells for Analysis of Therapeutic Tar-gets, Oncogenic Signaling Pathways and DNA Repair Markers. Cancers 2022, 14, 2810.

Contribution:

- establishment of the protocols for phospho–EGFR, γH2AX and PD–L1 /PD–L2 staining
- establishment of automated spot–counting mask (IDEAS software)
- processing of patient blood samples and subsequent CTC analysis
- analysis of data sets (CTC counting and analysis of PD–L1 /PD–L2 status)
- collection of patient characteristics and corresponding clinical data
- statistical analysis
- all figures and tables were created by Stephanie Staudte
    - Figure 1 is based on the established gating strategy for CTC detection
    - Figure 2A was created based on the statistical analysis of the recovery frequencies , Figure 2B corresponding representative images
    - Figure 3 was created based on the measured immune fluorescence intensities for each target and corresponding representative images
    - Table 1 summarizes the patient characteristics and the number of detected CTCs as well as PD–L1 /–L2 status, these data were collected based on the Charité documentation system and the corresponding CTC data were generated by statistical analysis
    - Figure 4 showing images of CTCs detected in patient blood samples
    - Figure 5 was generated by analysis of PD–L1 status of corresponding tumour tissue and liquid biopsy
    - Table 1, clinical data were collected for time points of biopsies and corresponding PD–L1 status

- Manuscript drafting, finalization and submission (Stephanie Staudte is corresponding author)

Publication 2:

Tinhofer, Ingeborg; **Staudte, Stephanie**, George, Stephen, Liquid biopsy in head neck cancer: ready for clinical routine diagnostics? Curr Opin Oncol 2023

Contribution

- Manuscript finalization

_____

Signature, date and stamp of first supervising university professor / lecturer

_____

Signature of doctoral candidate

Printing copy of the publication 1

cancers

MDPI

Artide

Multiparametric Phenotyping of Circulating Tumor Cells for Analysis of Therapeutic Targets, Oncogenic Signaling Pathways and DNA Repair Markers

Stephanie Staudte [1,2,*], Konrad Klinghammer [3,4], Philipp Sebastian Jurmeister [5,6], Paul Jank [7], Jens-Uwe Blohmer [8], Sandra Liebs [4], Peter Rhein [9], Anja E. Hauser [10,11] and Ingeborg Tinhofer [1,2]

1 Department of Radiooncology and Radiotherapy, Charité University Hospital, 10117 Berlin, Germany; ingeborg.tinhofer@charite.de
2 German Cancer Consortium (DKTK) Partner Site, and German Cancer Research Center (DKFZ), 69120 Heidelberg, Germany
3 Department of Hematology and Oncology, Charité University Hospital, 10117 Berlin, Germany; konrad.klinghammer@charite.de
4 Charité Comprehensive Cancer Center (CCCC), Charité University Hospital, 10117 Berlin, Germany; sandra.liebs@charite.de
5 Institute of Pathology, Charité University Hospital, 10117 Berlin, Germany; philipp.jurmeister@med.uni-muenchen.de
6 Institute of Pathology, Ludwig Maximilians University Hospital Munich, 80337 Munich, Germany
7 Institute of Pathology, Philipps-University Marburg and University-Hospital Marburg (UKGM), 35039 Marburg, Germany; paul.jank@uni-marburg.de
8 Breast Cancer Center, Charité University Hospital, 10117 Berlin, Germany; jens.blohmer@charite.de
9 Luminex B.V., A DiaSorin Company, 5215 MV 's-Hertogenbosch, The Netherlands; prhein@luminexcorp.com
10 Department of Rheumatology and Clinical Immunology, Charité University Hospital, 10117 Berlin, Germany; hauser@drfz.de
11 Deutsches Rheuma-Forschungszentrum (DRFZ), Leibniz Association, 10117 Berlin, Germany
* Correspondence: stephanie.staudte@charite.de

check for updates

Citation: Staudte, S.; Klinghammer, K.; Jurmeister, P.S.; Jank, P.; Blohmer, J.-U.; Liebs, S.; Rhein, P.; Hauser, A.E.; Tinhofer, I. Multiparametric Phenotyping of Circulating Tumor Cells for Analysis of Therapeutic Targets, Oncogenic Signaling Pathways and DNA Repair Markers. *Cancers* 2022, *14*, 2810. https://doi.org/10.3390/cancers14112810

Academic Editor: Noriyoshi Sawabata

Received: 9 May 2022
Accepted: 2 June 2022
Published: 6 June 2022

Publisher's Note: MDPI stays neutral with regard to jurisdictional claims in published maps and institutional affiliations.

Simple Summary: Detection of circulating tumor cells (CTCs) has been established as an independent prognostic marker in solid cancer. In order to expand the clinical utility of this blood–based minimally invasive biomarker we established a protocol allowing multiparametric phenotyping of CTCs to analyze the expression levels of therapeutic target proteins. By applying this assay, we demonstrated intratumoral heterogeneity of PD–L1 expression in CTCs from head and neck cancer patients, an observation previously reported in tumor tissue specimens. We further verified the feasibility of applying the protocol to analyze the activation status of important oncogenic pathways and the extent of DNA repair following radiation. These promising preliminary results warrant further study and may lead to the implementation of this assay in clinical routine for improved treatment selection and monitoring.

Abstract: Detection of circulating tumor cells (CTCs) has been established as an independent prognostic marker in solid cancer. Multiparametric phenotyping of CTCs could expand the area of application for this liquid biomarker. We evaluated the Amnis® brand ImageStream®X MkII (ISX) (Luminex, Austin, TX, USA) imaging flow cytometer for its suitability for protein expression analysis and monitoring of treatment effects in CTCs. This was carried out using blood samples from patients with head and neck squamous cell carcinoma (n = 16) and breast cancer (n = 8). A protocol for negative enrichment and staining of CTCs was established, allowing quantitative analysis of the therapeutic targets PD–L1 and phosphorylated EGFR (phospho–EGFR), and the treatment response marker γH2AX as an indicator of radiation–induced DNA damage. Spiking experiments revealed a sensitivity of 73% and a specificity of 100% at a cut–off value of ≥3 CTCs, and thus confirmed the suitability of the ISX-based protocol to detect phospho–EGFR and γH2AX foci in CTCs. Analysis of PD–L1/–L2 in both spiked and patient blood samples further showed that assessment of heterogeneity in protein expression within the CTC population was possible. Further validation of the

diagnostic potential of this ISX protocol for multiparametric CTC analysis in larger clinical cohorts is warranted.

Keywords: liquid biopsy; circulating tumor cells; imaging flow cytometry; Amnis®; multiparametric phenotyping; head and neck squamous cell carcinoma; breast cancer

1. Introduction

Circulating tumor cells (CTCs) represent the fraction of tumor cells which have detached from the tumor bulk and entered into blood circulation. Since they have the potential to travel to distant organs and seed new lesions, they are considered key players in metastasis formation [1]. The poor prognostic value of CTCs was first demonstrated in metastatic breast cancer [2] and was confirmed in subsequent studies in various solid cancers including colorectal [3], prostate [4], and head and neck cancer [5].

For the implementation of CTC detection as a blood–based biomarker in clinical routine, robust techniques for their enrichment and detection are prerequisites. The first system satisfying such requirements for use in clinical routine was the CellSearch® (CS) platform (Huntington Valley, PA, USA). This FDA–approved automated CTC detection system captures CTCs via magnetic beads coupled to an antibody specific for epithelial cell adhesion molecule (EpCAM) [6]. Although representing a highly sensitive device for patients with EpCAM high expressing tumors, the CS system has its limitations in tumors consisting of cells which have undergone partial or complete epithelial to mesenchymal transition (EMT) [7], thereby displaying reduced or absent EpCAM expression. Another limitation is the equipment of the CS system, which has only four fluorescence channels, thus making it unsuitable for comprehensive phenotyping of CTCs. This represents a major constraint for further development of CTC assays, such as their use for the identification of therapeutic targets, the short–term evaluation of therapy response and early detection of disease progression.

In the present study, we evaluated the suitability of the Amnis® ISX (Luminex, Austin, TX, USA), an imaging flow cytometer which can be equipped with up to ten fluorescence channels for CTC detection and multiparametric phenotyping. In addition to the assessment of sensitivity and specificity, we developed protocols for target identification (programmed cell death ligands 1 and 2 [PD–L1/–L2]; activated epidermal growth factor receptor; [EGFR]) and therapy response. For the latter, we focused on the assessment of the phosphorylated form of the histone 2a variant (γH2AX) as a surrogate marker of DNA repair efficacy after irradiation. As proof–of–concept, we used the ISX system for the analysis of blood samples from patients with head and neck squamous cell carcinoma (HNSCC) and breast cancer (BC).

2. Materials and Methods

2.1. Cell Lines

The cell lines used for spiking experiments were selected according to their expression levels of EpCAM and PD–L1/–L2. The cell lines SW620 (ATCC® CCL 227™, purchased from ATCC, Manassas, VA; USA) and UD–SCC–4 (University of Düsseldorf, NRW, Germany) were used to determine the sensitivity of the CTC assay. The MDA–MB–231 cell line (ATCC® HTB–26™, purchased from ATCC) was used to set the laser power and compensation matrix. For the establishment of the analysis of phospho–EGFR and γH2AX foci, UM–(University of Michigan, IL, USA)–SCC–22B, a gift from T.K. Hoffmann (University of Ulm, BW, Germany) [8] and the FaDu cell line (ATCC®HTB–43™, purchased from ATCC) were used, respectively. Cell cultures were maintained in a humidified incubator at 37 °C and 5% CO_2. The composition of cell culture media is described in Supplementary Table S1.

2.2. Blood Collection

For our pilot study, healthy donors (n = 7), as well as HNSCC (n = 16) and BC patients (n = 8) presenting at the Charité for tumor treatment were included. After obtaining informed consent, blood samples were collected in ethylenediaminetetraacetic acid (EDTA) coated vacutainer tubes (BD, NJ, USA) and stored at room temperature (RT) for at least 30 min before further processing.

2.3. Blood Sample Processing for CTC Enrichment

Blood samples were processed within four hours after blood withdrawal. Leukocyte depletion was performed using the RosetteSep™ Human CD45 Depletion Cocktail (Stemcell Technologies, Vancouver, BC, Canada) according to the manufacturer's instructions for 50 mL standard tubes. Briefly, after incubation with 50 µL of Depletion Cocktail per milliliter blood for 20 min at RT, blood was diluted with an equal volume of buffer composed of Dulbecco's Phosphate Buffered Saline (PBS; Gibco™, Waltham, MA, USA, cat. No. 14190–094) and 2% Fetal Bovine Serum (FBS; Gibco™, cat. No. 10270–106). Ficoll–Paque™ PLUS (Cytiva, Marlborough, MA, USA) was overlaid with diluted blood and centrifuged at 1200× g for 20 min at RT with the break off. The interphase, consisting of peripheral blood mononuclear cells (PBMCs) and CTCs/spiked tumor cells between plasma and ficoll, was harvested using a Pasteur pipette and directly transferred into a new 50 mL tube, which was then filled up with buffer (PBS/2%FBS). The washing procedure was performed twice and cells were centrifuged at 300× g for 10 min at RT with low break. Finally, the cell pellet was suspended in staining buffer (PBS/10%FCS) and transferred into a 5 mL FACS tube for further staining (Supplementary Figure S1).

2.4. Immune Fluorescence (IF) Staining

The following fluorescence–labelled antibodies were used for CTC phenotyping: AlexaFluor® 488 anti–human CD326 (EpCAM) Antibody (Biolegend, San Diego, CA, USA, cat. No. 324210, clone: 9C4, 1:100); AlexaFluor® 488 anti–human EGFR Antibody (Biolegend, cat. No. 352908, clone: AY13, 1:100); AlexaFluor® 647 anti–human CD45 Antibody (Biolegend, cat. No. 304018, clone: HI30, 1:50); APC/Fire™ 750 anti–human CD45 Antibody (Biolegend, cat. No. 304062, clone: HI30, 1:50); PE anti–human CD274 (B7H1, PD–L1) Antibody (Biolegend, cat. No. 393608, clone: MIH2, 1:20); PE–Vio® 770 anti–human CD273 (PD–L2) REAfinity™ Antibody (Miltenyi, Bergisch Gladbach, NRW, Germany, cat. No. 130–116–565, clone: REA985, 1:50).

After centrifugation of cell suspension at 300× g for 5 min at 4 °C, FcR Blocking reagent (Miltenyi, cat. No. 130–059–901, 1:10) was added and samples were incubated for 10 min. All further steps were performed protected from light. Cells were incubated with the directly fluorescence–conjugated antibodies for extracellular staining for 15 min at 4 °C. After washing with 2 mL of staining buffer, cells were fixed with 4% formaldehyde (Carl Roth, BW, Germany, cat. No. 4979.1, 1:9.25 dilution of 37% formaldehyde) for 15 min and counterstained with Hoechst 33342 (LifeTechnologies, Waltham, MA, USA, cat. No. H1399, 2 ng/mL) for 20 min.

For the establishment of the protocol for phospho–EGFR and γH2AX foci detection, cells were treated with 100 ng/mL EGF (Invitrogen, Waltham, MA, USA, cat. No. PHG0315) for 10 min at 37 °C and 5% CO_2 and/or irradiated with 2 Gray (Gy), respectively. After irradiation, cells were cultivated for 1 h and then harvested by trypsin treatment. For combined staining of surface and intracellular markers, the modified protocol of Durdik et al. [9] was used. Briefly, intracellular staining cells were fixed with 3% formaldehyde for 10 min at 4 °C, washed twice with 1 mL PBS, resuspended in 70% Ethanol and stored at −20 °C overnight. After an additional washing step, cells were permeabilized for 30 min at 4 °C by adding PBS supplemented with 1% BSA and 0.1% Triton X–100 (Th. Geyer, Renningen, BW, Germany). The following primary and secondary antibodies were used: Phospho–EGF Receptor (Tyr1068) (D7A5) XP® Rabbit mAb (Cell Signaling, Danvers, MA, USA, cat. No. 3777S, 1:1600); Texas Red–labelled goat anti–Rabbit IgG (Invitrogen, cat. No. T–2767,

4 µg/mL); AlexaFluor® 647 anti H2A.X Phospho–Ser139 Antibody (Biolegend, cat. No. 613408, clone: 2F3, 1.25 µg/mL). Samples were incubated with the primary antibodies for 2 h at RT. For secondary staining, cells were washed by centrifugation at 300× *g* for 5 min, resuspended in PBS and incubated with the antibody for 1 h at RT. After one additional washing step, cells were resuspended in 30 µL PBS and transferred into a 1.5 mL tube for imaging flow cytometric analysis.

2.5. Imaging Flow Cytometry—Amnis® ImageStream®X Mk II

The ISX equipped with lasers at 405 nm, 488 nm, 561 nm and 642 nm and the INSPIRE™ software (version 201.1.0.765; Luminex, Austin, TX, USA) was used for sample acquisition. Data analysis was performed with the IDEAS® software (version 6.2.187; Luminex, Austin, TX, USA). Cells were imaged at 40× magnification at low speed for receiving high–quality images with an acquisition time of 30 min per patient sample. The optimal compensation matrix between individual fluorescence channels was established using a mixture of MDA–MB–231 cells and PBMCs from a healthy donor, stained with each of the above–mentioned antibodies separately or in combination. The settings for acquisition and analysis were used for all samples (Supplementary Table S2).

2.6. Spiking Experiments

SW620 and UD–SCC–4 cells were harvested at a confluence of 90% by trypsin treatment. After cell counting using a conventional Neubauer Counting Chamber, aliquots of the cell suspension containing 500, 50 or 5 cells were prepared and added to 4 mL of blood from a healthy donor (blood–spiked samples) or to 4 mL of culture medium (reference samples). The blood–spiked samples were further processed using the RosetteSep™ Human CD45 Depletion Cocktail (Stemcell Technologies) as described above. Reference samples were used to calculate the recovery rate of the CTC assay. Staining and acquisition were performed as described above.

3. Results

3.1. Establishment of Multicolor CTC Detection

Since EpCAM expression was shown to be downregulated in squamous cell carcinomas [10], whereas EGFR is frequently overexpressed in HNSCC [11], we hypothesized that the inclusion of both tumor–associated markers may increase sensitivity for the detection of CTCs, especially in tumors with an EMT phenotype displaying low or absent EpCAM expression. After identifying the optimal antibody concentrations, the following gating strategy was developed (Figure 1): after the exclusion of speedbeads and debris, a gate was set on Hoechst^{positive} nucleated cells and fluorescence intensities of CD45–AF647 and EpCAM–EGFR–AF488 were visualized in a 2D dot plot. CTCs were detected within the CD45^{negative}/EpCAM–EGFR^{positive} gate or, when clustered to leukocytes, in the CD45^{positive}/EpCAM–EGFR^{positive} gate. This CTC gating strategy was then applied to all subsequent experiments.

Spiking experiments were performed to investigate the sensitivity and specificity of the ISX–based assay. The procedure of the spiking experiments, including staining for CTC detection and ISX acquisition, is described in the Material and Methods section. Recovery frequencies (%–RF) were calculated by dividing the number of tumor cells detected in the blood–spiked sample by the number of tumor cells detected in the reference sample, multiplied by 100. The median recovery of three independent technical replicates of spiked SW620 cells was 73%. Overall, a correlation of $R^2 = 0.96$ (SW620) was observed for recoveries from spiking samples (Figure 2A). Similar results were received for UD–SCC–4 ($R^2 = 0.92$; Supplementary Figure S2). We also confirmed that our protocol allowed for a clear discrimination between single CTCs (Hoechst^{positive}/EpCAM–EGFR^{positive}/CD45^{negative}) and CTC–leukocyte clusters (Hoechst^{positive}/EpCAM–EGFR^{positive}/CD45^{positive}) (Figure 2B).

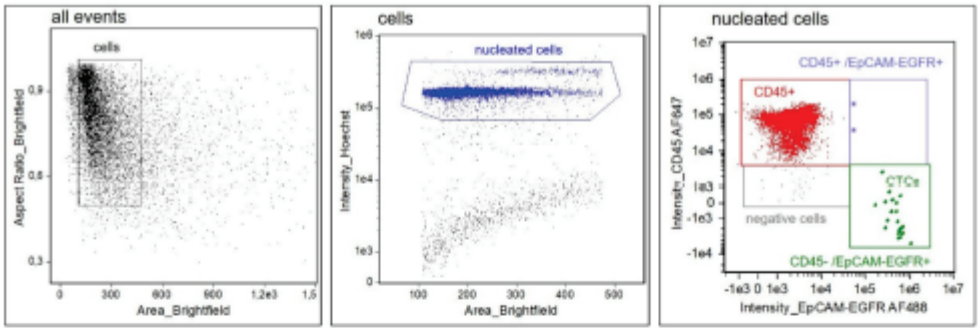

Figure 1. Gating strategy for CTC detection. At first, speedbeads and debris are excluded. Hoechst staining intensity of the gated events is displayed in a 2D plot. Hoechst^{positive} nucleated cells (blue) are then separated by their fluorescence intensities for EpCAM–EGFR–AF488 and CD45–AF647. CTCs are defined as Hoechst^{positive}/CD45^{negative}/EpCAM–EGFR^{positive}. Single CTCs are detected in the CD45^{negative}/EpCAM–EGFR^{positive} gate (green), whereas cluster of leukocytes and CTCs are detected in the CD45^{positive}/EpCAM–EGFR^{positive} gate (purple).

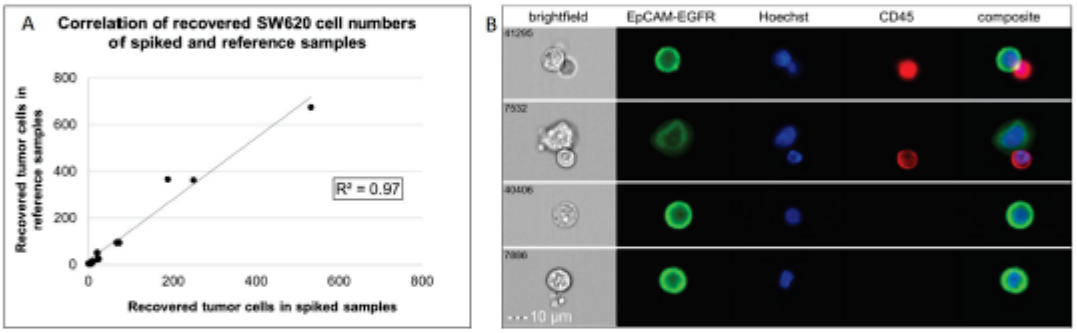

Figure 2. Detection of spiked SW620 cells by imaging flow cytometry. (**A**) Analysis of samples (n = 3 replicates per dilution) revealed a correlation of R^2 = 0.97 of recovered cells in reference and spiked samples. (**B**) Representative images from a spiking experiment.

Blinded analysis of blood samples (n = 11) from healthy donors (n = 7) was performed in order to determine the specificity of the CTC detection assay. For a positive control, 500 UD–SCC–4 cells were spiked into a blood sample immediately before sample blinding. Staining and ISX analysis were performed as described above. Subsequently, in 1 of the 11 healthy donor samples (9%), two EpCAM–EGFR^{positive} cells were detected. Thus, without applying a threshold, a specificity of 91% was achieved by our protocol. A specificity of 100% was obtained when applying the cut–off value of ≥3 CTCs, a threshold previously associated with a significantly worse outcome in metastatic colon cancer [3].

3.2. *Phenotyping of CTCs*

The ISX–based protocol was further developed for multiparametric phenotyping of CTCs. Considering their important role as therapeutic targets in various epithelial tumor entities, EGFR in its phosphorylated activated form (phospho–EGFR) and the two immune checkpoints PD–L1 and PD–L2 were included in the marker panel. In addition, for analysis of residual DNA double strand breaks as a potential marker of radioresistant CTCs emigrating from the irradiated field, we also included detection of the phosphorylated form of the histone 2a variant (γH2AX) to our multiparametric panel.

In the first step, the staining was set up for each single marker. Phospho–EGFR staining was established using the UM–SCC–22B cell line displaying high EGFR expression

levels. Cells were left untreated (negative control) or were treated with EGF (positive control). PD–L1/–L2 staining was established with the cell lines MDA–MB–231 (PD–L1^{positive} PD–L2^{weak}) and SCC–25 (PD–L1^{weak} PD–L2^{positive}). For establishment of γH2AX foci staining, FaDu cells were left untreated (negative control), or were irradiated with a single dose of 2 Gy or 10 Gy (positive controls). Isotype controls were included for assessment of background signals, except for phospho–EGFR staining in which staining with the secondary antibody alone was used to determine unspecific signals.

Analysis of each marker individually confirmed that a clear discrimination of untreated and EGF–treated (Figure 3A) and PD–L1/–L2 negative versus positive cells was possible (Figure 3B,C). In line with the successful detection of DNA double strand breaks, a dose–dependent increase in the number of γH2AX foci (Supplementary Figure S3) and in the nuclear γH2AX signal intensity was observed in irradiated compared to non–irradiated cells (Figure 3D). The whole antibody panel was validated by spiking FaDu cells, which had previously been irradiated and treated with EGF, into blood samples from a healthy donor. The suitability of our protocol for parallel analysis of EGFR signaling activity, immune checkpoint expression and DNA damage response was thereby confirmed (Figure 3E).

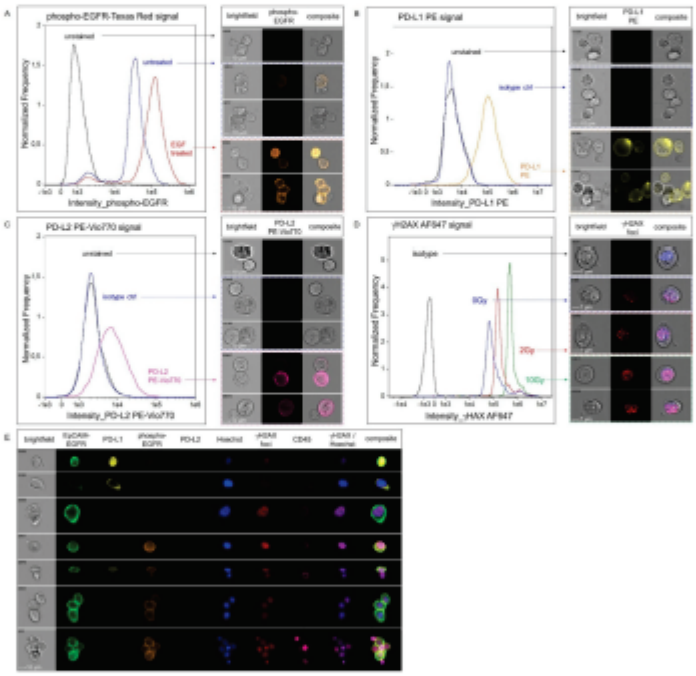

Figure 3. Immunofluorescence analysis of phospho–EGFR, PD–L1/PD–L2 and γH2AX and multi-parametric phenotyping. (**A**) Representative results of phospho–EGFR staining in UM–SCC–22B cells are shown. The histogram displays the fluorescence intensities in unstained (black), untreated (blue) and EGF–treated (red) cells. (**B**,**C**) Positive and negative cells for surface staining of PD–L1 (B) and PD–L2 (C) on MDA–MB–231 and SCC–25 cells, respectively, are shown. Fluorescence intensities for unstained (black), isotype control (blue) or samples stained with either anti–PD–L1 (orange) or anti–PD–L2 antibody (pink) are depicted. Clusters of cells were selected to demonstrate the heterogeneity of each cell line and the feasibility of the ISX to detect different expression intensities with high sensitivity. (**D**) γH2AX staining was performed in FaDu cells, untreated (blue) or irradiated with 2 Gy (red) or 10 Gy (green). Isotype control is shown in black. Representative images for the different conditions (acquired with the 60× objective at low speed) are presented at the right column of the figure. (**E**) Multiparametric phenotyping of spiked EGF–treated and irradiated FaDu cells in peripheral blood (acquired with 40× magnification).

3.3. Assessment of CTCs in Blood Samples from Patients with HNSCC and BC

In order to test the suitability of our ISX protocol for multiparametric CTC phenotyping in patients with epithelial cancer, blood samples from patients with HNSCC (n = 16) and BC (n = 8) were used. Patient characteristics are presented in Table 1.

Table 1. Patient characteristics.

		HNSCC	BC
gender			
n	female	4	8
	male	12	-
age (years) median (range)			
	female	70 (32–81)	48 (34–64)
	male	69 (58–79)	-
stage of disease n (%)			
	early stage	-	4 (50%)
	locally advanced	1 (6%)	-
	recurrent/metastatic	15 (94%)	4 (50%)
tumor site n (%)			
	oral cavity	8 (50%)	-
	oropharynx	3 (19%)	-
	hypopharynx	3 (19%)	-
	other/breast	2 (12%)	8 (100%)
metastatic sites n (%)			
	none	1 (0.06%)	4 (50%)
	regional	3 (25%)	3 (38%)
	distant	12 (75%)	1(12%)
$CTC^{positive}$ cases ($\geq$ 3 CTCs) n (%)		7 (44%)	6 (75%)
	CTC numbers		
	median	15	14
	range	6–30	9–27
$PD\text{-}L1^{positive}$ cases n (%)		4 (57%)	4 (67%)
	$PD\text{-}L1^{positive}$ cells		
	median (n)	6	2
	range (n)	3–30	1–6
% of $PD\text{-}L1^{positive}$ CTCs in entire CTC population	median (%)	100%	15%
	range (%)	56%–100%	4%–25%

Applying the protocol for surface marker analysis and using a cut–off value for CTC–positivity of $\geq$3 CTCs, 7 out of 16 HNSCC patients tested positive for CTCs. In 4 of the $CTC^{positive}$ cases PD–L1 expressing CTCs were detected and the amount of $PD\text{–}L1^{positive}$ CTCs ranged from 56% to 100%. In the BC cohort, $\geq$3 CTCs were found in 6 out of 8 patients. Here, PD–L1 expression was detectable in 67% of the $CTC^{positive}$ cases. Its expression varied from being absent to high within individual samples (Figure 4).

In the light of the substantial inter– and intrapatient tumoral heterogeneity in PD–L1 expression in CTCs, we next determined the correlation between liquid and tumor biopsies. Paired analysis of PD–L1 expression on CTCs and the corresponding tumor tissue in seven cases (HNSCC n = 5; BC n = 2) revealed a weak correlation (R^2 = 0.22; Figure 5).

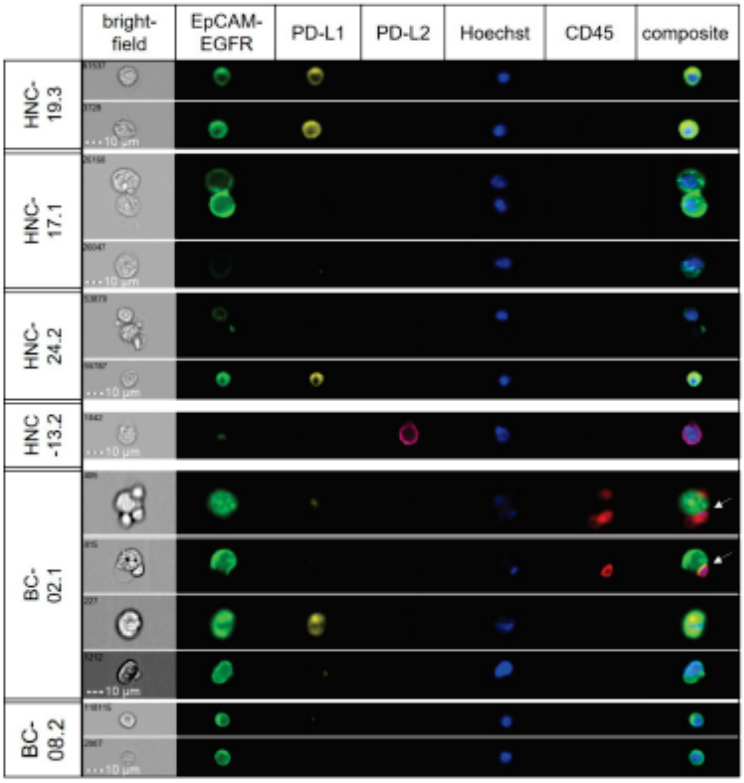

Figure 4. Detection of intratumoral heterogeneity in marker expression in CTCs. Representative images from selected patient samples (head and neck; HNC), showing varying expression levels of target proteins. In one case (BC–02.1), clusters of CTCs and leukocytes were observed (white arrows).

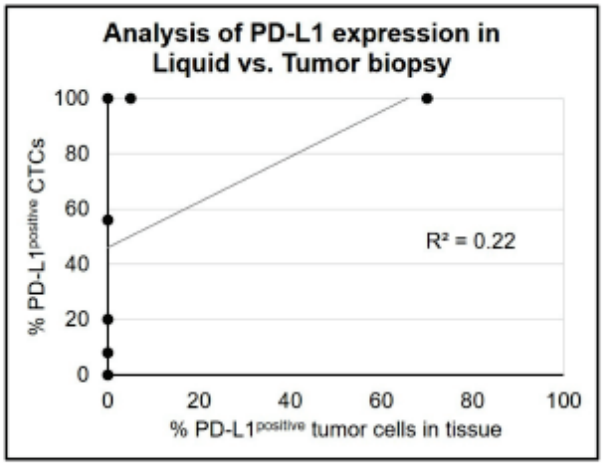

Figure 5. Paired analysis of PD–L1 expression in tumor tissue and liquid biopsy. Cases with ≥3 CTCs detected at baseline were used for paired analysis of PD–L1 expression analysis in tumor tissue and corresponding liquid biopsy. (pairs $n = 7$; BC: $n = 2$, HNSCC: $n = 5$).

A concordance between tumor tissue and liquid biopsy was found in four cases, where in two patients with PD–L1 expressing tissues (tumor proportion score 5% and 70%) all corresponding CTCs were PD–L1^{positive}. The other two concordant cases were negative for PD–L1 in both sample types. The remaining cases had detectable PD–L1 expression on CTCs, but the corresponding tumor tissue was tested negative for PD–L1. The median time between tissue collection and liquid biopsy was 4.6 months (range 0.4 –19 months, Table 2), where the conventional biopsy was carried out first.

Table 2. PD–L1 expression in tumor tissue and CTCs. Results from cases with ≥ 3 CTCs and available matched tumor tissue are presented. Concordant cases are highlighted in green (TPS: tumor proportion score).

Pat.ID	Tumor Site	Date of tissue Biopsy (Month/Year)	Date of Liquid Biopsy (Month/Year)	PD–L1^{positive} Cells in Tumor Tissue (TPS %)	PD–L1^{positive} CTCs (%)	Time between Tumor and Liquid Biopsy (Months)
BC-003	breast	December/2017	December /2017	0	8	0.4
BC-006	breast	December /2017	January/2018	0	20	1
HNC-012	oral cavity	September/2017	September /2017	70	100	0.4
HNC-018	oral cavity	July/2016	January /2018	0	0	19
HNC-019	oral cavity	September /2017	January /2018	0	45	5
HNC-020	hypopharynx	January/2017	January /2018	5	100	12
HNC-026	hypopharynx	December /2016	Mar./2018	0	0	15

4. Discussion

To date, only a few studies have assessed the suitability of the ISX system for CTC detection [12–16]. In the current study, we could extend this limited evidence and show that sensitive and specific CTC detection is feasible by using this platform. Spiking experiments with our ISX protocol showed a median recovery rate of 73%, which was similar to the ISX–based CTC study of Ruiz-Rodríguez et al. [12], and even slightly better compared to other ISX–based studies showing recovery rates from 44% to 55%, respectively [13,14]. We did not compare the performance of the ISX with the CS system on corresponding patient samples. Evidence from the literature, however, strongly supports equivalent performance of both platforms, which is also underlined by results from a head–to–head comparison in the study of López–Riquelme et al. [17]. Using blood samples spiked with the pancreatic cancer cell line PANC–1 and staining for the tumor–cell markers EpCAM and cytokeratin, similar detection rates for the CS and ISX systems were observed at spiked cell numbers >10 [17]. In contrast to this study, where lower sensitivity of the ISX was reported for ≤10 spiked cells, we observed robust detection of spiked tumor cells even at a minimum of 5 cells per 4 mL blood. Combined staining of EpCAM and EGFR as tumor–associated markers might explain the high sensitivity of our ISX protocol.

Without applying a cut–off for CTC positivity, the specificity of our ISX protocol was 91%, where 1 of 11 samples tested positive in a blinded analysis of healthy donor blood samples. While the optimal cut–off for definition of a poor–outcome group has yet to be established in HNSCC [5,18], a cut–off of ≥3 CTCs/7.5 mL blood has been demonstrated to identify colon cancer patients with poor outcomes [3]. Using this threshold, specificity increased to 100% for our CTC detection protocol. Again, this high specificity is in line with the results from previous ISX–based CTC studies [14,16].

We further demonstrated that the ISX platform can be exploited for quantitative analysis of EGFR pathway activity in CTCs. Inclusion of phospho–EGFR in multiparametric CTC analysis is promising given the interference of EGFR signaling with DNA repair [19] and radioresistance [20]. Furthermore, Serrano et al. have shown that EGFR^{positive} CTCs co-express EMT markers, indicative of a high metastatic potential of this CTC subpopulation [21]. Induction of EMT by radiotherapy has been suggested as the underlying mechanism of the increase in CTC numbers observed in patients treated with radiother-

apy [22]. Assessment of γH2AX foci as a marker of radiation–induced DNA double strand breaks [23] using our ISX protocol might represent an interesting biomarker by allowing for a discrimination between CTCs derived from the bulk tumor treated by radiotherapy and those originating from micrometastases outside of the irradiated field. By spiking experiments with irradiated and non–irradiated cells, we showed that the semi–automated quantification of dose–dependent effects of radiation in CTCs is possible by using our protocol. Dynamic assessment of viable CTCs derived from the radiation field and persisting during radiotherapy may not only identify radioresistant tumors [24–26] but could also guide the clinical development of combined therapies with radiosensitizing drugs [27,28].

Immune checkpoint inhibitors (ICIs) are currently developed in the curative and recurrent/metastatic setting. Immunohistochemical staining of PD–L1 in tumor tissue has been established as a predictive marker of treatment efficacy of PD–1 inhibitors. However, intratumoral heterogeneity in PD–L1 expression [29,30] can limit the accuracy of this biomarker, and could explain why some patients with PD–L1^{negative} tumors respond to ICIs while others with PD–L1 expressing tumors do not benefit from this treatment [31,32]. Thus, complementary analysis of PD–L1 expression in tumor and liquid biopsies could improve the predictive value of PD–L1. Preliminary evidence from the analysis of PD–L1 in CTCs in melanoma [32] and non–small cell lung cancer (NSCLC) [33,34] supports this hypothesis. In melanoma, detection of PD–L1^{positive} CTCs at baseline was associated with a significantly longer progression–free survival after pembrolizumab treatment [32]. A similar observation was reported for patients with NSCLC treated with nivolumab [34]. In both studies, intrapatient heterogeneity of PD–L1 expression in CTCs, and a low to moderate correlation between PD–L1 status of CTCs and tumor tissue, were reported, in line with the preliminary results of our study. In contrast, while basal PD–L1^{positive} CTC numbers were not associated with nivolumab efficacy in a study of advanced NSCLC, their persistence after treatment identified patients with decreased progression-free survival [35,36]. This negative prognostic value of the presence of PD–L1 expressing CTCs after treatment was also shown by Tan et al. in a mixed cohort of patients with advanced cancers [37]. In addition to the accumulating evidence of a positive correlation between baseline PD–L1^{positive} CTCs and the response to ICI treatment, a negative association with survival after treatment with other non–ICI regimes has been demonstrated in HNSCC [36] and NSCLC [38].

We confirmed the applicability of our assay in a small cohort of HNSCC ($n = 16$) and BC ($n = 8$) patients. The application of a cut–off value for CTC–positivity of ≥ 3 CTCs resulted in 7 out of 16 (44%) HNSCC patients being classified as CTC^{positive} at baseline. Similar detection rates by the CS system have been reported from previous HNSCC studies [5,39]. Among the seven CTC^{positive} cases, 57% had PD–L1 expressing CTCs. This was higher than reported by Strati et al. who could detect PD–L1 expression in 12% of the CTC^{positive} cases [36], however, the small size of the cohorts did not allow a statistical comparison of the two studies.

Concordance between PD–L1 expression in tumor tissue and CTCs was weak in our study. Discrepant results were reported for lung cancer, ranging from no/low [33,40] to high concordance [41]. A low correlation of PD–L1 expression in tumor tissue and liquid biopsy could be due to spatial heterogeneity [29,30,42] and/or dynamic changes in PD–L1 expression in tumors which cannot be captured by a single tissue biopsy. Also, the impact of time and/or treatment applied between tissue and liquid biopsy collection on the concordance of PD–L1 expression remains unclear. Future studies that include larger patient numbers will certainly be needed to establish the extent of intratumoral heterogeneity in PD–L1 expression and the complementary value of CTC–based PD–L1 analysis as a predictive marker of ICI efficacy.

Indeed, one major limitation of our study was the small number of patient samples. In order to establish the predictive and prognostic value of the CTC biomarker panel, analyses in larger cohorts of HNSCC patients with locally advanced disease treated with radiotherapy as well as recurrent/metastatic disease treated with anti PD–1 antibodies are

planned. In future studies, we will also include the analysis of intracellular/nuclear PD–L1 expression, given the preliminary evidence of its interference with radiosensitivity [43] and outcome [44]. In addition, algorithms for the semi–automated quantification of CTCs with an activated EGFR pathway phenotype and γH2AX foci counting [9] will be optimized to further reduce intra- and interobserver variability of CTC analysis.

5. Conclusions

We successfully established a specific and sensitive assay for the detection and multiparametric phenotyping of CTCs using the Amnis® ImageStream®X Mk II. We demonstrated the feasibility of our protocol for the analysis of intratumoral heterogeneity of PD–L1 expression, EGFR activation and the DNA damage repair in CTCs.

Supplementary Materials: The following supporting information can be downloaded at: https://www.mdpi.com/article/10.3390/cancers14112810/s1. Supplementary Table S1: Media composition used for cultivation of the mentioned cell lines. Supplementary Figure S1: Workflow of the CTC analysis. Supplementary Table S2: Laser settings. Supplementary Figure S2: Results from spiking experiments using the UD–SCC–4 cell line. Supplementary Figure S3: Quantitative analysis of γH2AX foci.

Author Contributions: Conceptualization I.T. and S.L.; methodology S.S.; discussion and planning of experimental set up S.S. and S.L.; patient recruitment K.K. and J.-U.B.; technical support and ISX supervision P.R. and A.E.H.; pathological preparation and analysis of FFPE by P.S.J. and P.J.; Writing of the original draft: S.S. and I.T.; Review and editing by I.T. and S.S. All authors have read and agreed to the published version of the manuscript.

Funding: This study was financed by a grant within the German Cancer Consortium (to I.T. and S.L.). The DKTK is funded as one of the National German Health Centers by the Federal German Ministry of Education and Research. Additional funding was received from the Berliner Krebsgesellschaft (TIFF201822; I.T.). A.E.H. was funded by the Einstein Stiftung Berlin (A–2019–559).

Institutional Review Board Statement: The study was conducted in accordance with the Declaration of Helsinki and was approved by the Ethics Committee of the Charité University Hospital (EA1/152/10).

Informed Consent Statement: The Ethics Committee of the Charité University Hospital approved this study (EA1/152/10). Written informed consent has been obtained from the patients.

Data Availability Statement: The data that support the findings of this study are available from the corresponding author upon reasonable request.

Acknowledgments: We are grateful to the patients for their participation in this study. We also would like to acknowledge the participation of Stephen George for English language editing.

Conflicts of Interest: There are no conflicts of interest to be declared.

References

1. Lozar, T.; Gersak, K.; Cemazar, M.; Kuhar, C.G.; Jesenko, T. The biology and clinical potential of circulating tumor cells. *Radiol. Oncol.* **2019**, *53*, 131–147. [CrossRef] [PubMed]
2. Cristofanilli, M.; Budd, G.T.; Ellis, M.J.; Stopeck, A.; Matera, J.; Miller, M.C.; Reuben, J.M.; Doyle, G.V.; Allard, W.J.; Terstappen, L.W.; et al. Circulating tumor cells, disease progression, and survival in metastatic breast cancer. *N. Engl. J. Med.* **2004**, *351*, 781–791. [CrossRef] [PubMed]
3. Cohen, S.J.; Punt, C.J.; Iannotti, N.; Saidman, B.H.; Sabbath, K.D.; Gabrail, N.Y.; Picus, J.; Morse, M.; Mitchell, E.; Miller, M.C.; et al. Relationship of circulating tumor cells to tumor response, progression-free survival, and overall survival in patients with metastatic colorectal cancer. *J. Clin. Oncol.* **2008**, *26*, 3213–3221. [CrossRef] [PubMed]
4. Lorente, D.; Olmos, D.; Mateo, J.; Bianchini, D.; Seed, G.; Fleisher, M.; Danila, D.C.; Flohr, P.; Crespo, M.; Figueiredo, I.; et al. Decline in Circulating Tumor Cell Count and Treatment Outcome in Advanced Prostate Cancer. *Eur. Urol.* **2016**, *70*, 985–992. [CrossRef] [PubMed]
5. Grisanti, S.; Almici, C.; Consoli, F.; Buglione, M.; Verardi, R.; Bolzoni-Villaret, A.; Bianchetti, A.; Ciccarese, C.; Mangoni, M.; Ferrari, L.; et al. Circulating tumor cells in patients with recurrent or metastatic head and neck carcinoma: Prognostic and predictive significance. *PLoS ONE* **2014**, *9*, e103918. [CrossRef]

6. Allard, W.J.; Matera, J.; Miller, M.C.; Repollet, M.; Connelly, M.C.; Rao, C.; Tibbe, A.G.; Uhr, J.W.; Terstappen, L.W. Tumor cells circulate in the peripheral blood of all major carcinomas but not in healthy subjects or patients with nonmalignant diseases. *Clin. Cancer Res.* **2004**, *10*, 6897–6904. [CrossRef]
7. Tayoun, T.; Faugeroux, V.; Oulhen, M.; Aberlenc, A.; Pawlikowska, P.; Farace, F. CTC-Derived Models: A Window into the Seeding Capacity of Circulating Tumor Cells (CTCs). *Cells* **2019**, *8*, 1145. [CrossRef]
8. Holz, C.; Niehr, F.; Boyko, M.; Hristozova, T.; Distel, L.; Budach, V.; Tinhofer, I. Epithelial-mesenchymal-transition induced by EGFR activation interferes with cell migration and response to irradiation and cetuximab in head and neck cancer cells. *Radiother. Oncol.* **2011**, *101*, 158–164. [CrossRef]
9. Durdik, M.; Kosik, P.; Gursky, J.; Vokalova, L.; Markova, E.; Belyaev, I. Imaging flow cytometry as a sensitive tool to detect low-dose-induced DNA damage by analyzing 53BP1 and γH2AX foci in human lymphocytes. *Cytometry A* **2015**, *87*, 1070–1078. [CrossRef]
10. Keller, L.; Werner, S.; Pantel, K. Biology and clinical relevance of EpCAM. *Cell Stress* **2019**, *3*, 165–180. [CrossRef]
11. Rivera, F.; García-Castaño, A.; Vega, N.; Vega-Villegas, M.E.; Gutiérrez-Sanz, L. Cetuximab in metastatic or recurrent head and neck cancer: The EXTREME trial. *Expert Rev. Anticancer Ther.* **2009**, *9*, 1421–1428. [CrossRef]
12. Ruiz-Rodríguez, A.J.; Molina-Vallejo, M.P.; Aznar-Peralta, I.; González Puga, C.; Cañas García, I.; González, E.; Lorente, J.A.; Serrano, M.J.; Garrido-Navas, M.C. Deep Phenotypic Characterisation of CTCs by Combination of Microfluidic Isolation (IsoFlux) and Imaging Flow Cytometry (ImageStream). *Cancers* **2021**, *13*, 6386. [CrossRef]
13. Chudasama, D.; Katopodis, P.; Stone, N.; Haskell, J.; Sheridan, H.; Gardner, B.; Urnovitz, H.; Schuetz, E.; Beck, J.; Hall, M.; et al. Liquid Biopsies in Lung Cancer: Four Emerging Technologies and Potential Clinical Applications. *Cancers* **2019**, *11*, 331. [CrossRef]
14. Dent, B.M.; Ogle, L.F.; O'Donnell, R.L.; Hayes, N.; Malik, U.; Curtin, N.J.; Boddy, A.V.; Plummer, E.R.; Edmondson, R.J.; Reeves, H.L.; et al. High-resolution imaging for the detection and characterisation of circulating tumour cells from patients with oesophageal, hepatocellular, thyroid and ovarian cancers. *Int. J. Cancer* **2016**, *138*, 206–216. [CrossRef]
15. Takahashi, Y.; Shirai, K.; Ijiri, Y.; Morita, E.; Yoshida, T.; Iwanaga, S.; Yanagida, M. Integrated system for detection and molecular characterization of circulating tumor cells. *PLoS ONE* **2020**, *15*, e0237506. [CrossRef]
16. Ogle, L.F.; Orr, J.G.; Willoughby, C.E.; Hutton, C.; McPherson, S.; Plummer, R.; Boddy, A.V.; Curtin, N.J.; Jamieson, D.; Reeves, H.L. Imagestream detection and characterisation of circulating tumour cells—A liquid biopsy for hepatocellular carcinoma? *J. Hepatol.* **2016**, *65*, 305–313. [CrossRef]
17. López-Riquelme, N.; Minguela, A.; Villar-Permuy, E.; Ciprian, D.; Castillejo, A.; Álvarez-López, M.R.; Soto, J.L. Imaging cytometry for counting circulating tumor cells: Comparative analysis of the CellSearch vs ImageStream systems. *Apmis* **2013**, *121*, 1139–1143. [CrossRef]
18. Harris, E.J.; Huang, J.; Carroll, E.; Lowe, A.C.; Chau, N.G.; Rabinowits, G.; Haddad, R.; Hanna, G.J.; Haddad, T.; Sanborn, M.; et al. Circulating tumor cell analysis in locally advanced and metastatic squamous cell carcinoma of the head and neck. *Laryngoscope Investig. Otolaryngol.* **2020**, *5*, 1063–1069. [CrossRef]
19. Rodemann, H.P.; Dittmann, K.; Toulany, M. Radiation-induced EGFR-signaling and control of DNA-damage repair. *Int. J. Radiat. Biol.* **2007**, *83*, 781–791. [CrossRef]
20. Ang, K.K.; Berkey, B.A.; Tu, X.; Zhang, H.Z.; Katz, R.; Hammond, E.H.; Fu, K.K.; Milas, L. Impact of epidermal growth factor receptor expression on survival and pattern of relapse in patients with advanced head and neck carcinoma. *Cancer Res.* **2002**, *62*, 7350–7356.
21. Serrano, M.J.; Alvarez-Cubero, M.J.; De Miguel Pérez, D.; Rodriguez-Martinez, A.; Gonzalez-Herrera, L.; Robles-Fernandez, I.; Hernandez, J.E.; Puche, J.L.G.; Lorente, J.A. Significance of EGFR Expression in Circulating Tumor Cells. *Adv. Exp. Med. Biol.* **2017**, *994*, 285–296. [CrossRef]
22. Tinhofer, I.; Hristozova, T.; Stromberger, C.; Keilholz, U.; Budach, V. Monitoring of circulating tumor cells and their expression of EGFR/phospho-EGFR during combined radiotherapy regimens in locally advanced squamous cell carcinoma of the head and neck. *Int. J. Radiat. Oncol. Biol. Phys.* **2012**, *83*, e685–e690. [CrossRef]
23. Carusillo, A.; Mussolino, C. DNA Damage: From Threat to Treatment. *Cells* **2020**, *9*, 1665. [CrossRef]
24. Martin, O.A.; Anderson, R.L.; Russell, P.A.; Cox, R.A.; Ivashkevich, A.; Swierczak, A.; Doherty, J.P.; Jacobs, D.H.; Smith, J.; Siva, S.; et al. Mobilization of viable tumor cells into the circulation during radiation therapy. *Int. J. Radiat. Oncol. Biol. Phys.* **2014**, *88*, 395–403. [CrossRef]
25. Martin, O.A.; Anderson, R.L.; Narayan, K.; MacManus, M.P. Does the mobilization of circulating tumour cells during cancer therapy cause metastasis? *Nat. Rev. Clin. Oncol.* **2017**, *14*, 32–44. [CrossRef]
26. Vilalta, M.; Rafat, M.; Graves, E.E. Effects of radiation on metastasis and tumor cell migration. *Cell. Mol. Life Sci.* **2016**, *73*, 2999–3007. [CrossRef]
27. Adams, D.L.; Adams, D.K.; He, J.; Kalhor, N.; Zhang, M.; Xu, T.; Gao, H.; Reuben, J.M.; Qiao, Y.; Komaki, R.; et al. Sequential Tracking of PD-L1 Expression and RAD50 Induction in Circulating Tumor and Stromal Cells of Lung Cancer Patients Undergoing Radiotherapy. *Clin. Cancer Res.* **2017**, *23*, 5948–5958. [CrossRef]
28. Wang, Y.; Liu, Z.G.; Yuan, H.; Deng, W.; Li, J.; Huang, Y.; Kim, B.Y.S.; Story, M.D.; Jiang, W. The Reciprocity between Radiotherapy and Cancer Immunotherapy. *Clin. Cancer Res.* **2019**, *25*, 1709–1717. [CrossRef]

29. Gniadek, T.J.; Li, Q.K.; Tully, E.; Chatterjee, S.; Nimmagadda, S.; Gabrielson, E. Heterogeneous expression of PD-L1 in pulmonary squamous cell carcinoma and adenocarcinoma: Implications for assessment by small biopsy. *Mod. Pathol.* **2017**, *30*, 530–538. [CrossRef]
30. Rasmussen, J.H.; Lelkaitis, G.; Håkansson, K.; Vogelius, I.R.; Johannesen, H.H.; Fischer, B.M.; Bentzen, S.M.; Specht, L.; Kristensen, C.A.; von Buchwald, C.; et al. Intratumor heterogeneity of PD-L1 expression in head and neck squamous cell carcinoma. *Br. J. Cancer* **2019**, *120*, 1003–1006. [CrossRef]
31. Ferris, R.L.; Blumenschein, G., Jr.; Fayette, J.; Guigay, J.; Colevas, A.D.; Licitra, L.; Harrington, K.; Kasper, S.; Vokes, E.E.; Even, C.; et al. Nivolumab for Recurrent Squamous-Cell Carcinoma of the Head and Neck. *N. Engl. J. Med.* **2016**, *375*, 1856–1867. [CrossRef] [PubMed]
32. Khattak, M.A.; Reid, A.; Freeman, J.; Pereira, M.; McEvoy, A.; Lo, J.; Frank, M.H.; Meniawy, T.; Didan, A.; Spencer, L.; et al. PD-L1 Expression on Circulating Tumor Cells May Be Predictive of Response to Pembrolizumab in Advanced Melanoma: Results from a Pilot Study. *Oncologist* **2020**, *25*, e520–e527. [CrossRef] [PubMed]
33. Janning, M.; Kobus, F.; Babayan, A.; Wikman, H.; Velthaus, J.-L.; Bergmann, S.; Schatz, S.; Falk, M.; Berger, L.-A.; Böttcher, L.-M.; et al. Determination of PD-L1 Expression in Circulating Tumor Cells of NSCLC Patients and Correlation with Response to PD-1/PD-L1 Inhibitors. *Cancers* **2019**, *11*, 835. [CrossRef] [PubMed]
34. Shibaki, R.; Koh, Y.; Akamatsu, H.; Kurita, K.; Yagi, S.; Kanai, K.; Hayata, A.; Tokudome, N.; Higuchi, M.; Kanbara, H.; et al. Predictive impact of PD-L1-expressing circulating tumor cells in NSCLC patients treated with nivolumab. *J. Clin. Oncol.* **2017**, *35*, 11541. [CrossRef]
35. Nicolazzo, C.; Raimondi, C.; Mancini, M.; Caponnetto, S.; Gradilone, A.; Gandini, O.; Mastromartino, M.; Del Bene, G.; Prete, A.; Longo, F.; et al. Monitoring PD-L1 positive circulating tumor cells in non-small cell lung cancer patients treated with the PD-1 inhibitor Nivolumab. *Sci. Rep.* **2016**, *6*, 31726. [CrossRef] [PubMed]
36. Strati, A.; Koutsodontis, G.; Papaxoinis, G.; Angelidis, L.; Zavridou, M.; Economopoulou, P.; Kotsantis, I.; Avgeris, M.; Mazel, M.; Perisanidis, C.; et al. Prognostic significance of PD-L1 expression on circulating tumor cells in patients with head and neck squamous cell carcinoma. *Ann. Oncol.* **2017**, *28*, 1923–1933. [CrossRef]
37. Tan, Z.; Yue, C.; Ji, S.; Zhao, C.; Jia, R.; Zhang, Y.; Liu, R.; Li, D.; Yu, Q.; Li, P.; et al. Assessment of PD-L1 Expression on Circulating Tumor Cells for Predicting Clinical Outcomes in Patients with Cancer Receiving PD-1/PD-L1 Blockade Therapies. *Oncologist* **2021**, *26*, e2227–e2238. [CrossRef]
38. Man, J.; Millican, J.; Mulvey, A.; Gebski, V.; Hui, R. Response Rate and Survival at Key Timepoints With PD-1 Blockade vs Chemotherapy in PD-L1 Subgroups: Meta-Analysis of Metastatic NSCLC Trials. *JNCI Cancer Spectr.* **2021**, *5*, pkab012. [CrossRef]
39. Kulasinghe, A.; Perry, C.; Warkiani, M.E.; Blick, T.; Davies, A.; O'Byrne, K.; Thompson, E.W.; Nelson, C.C.; Vela, I.; Punyadeera, C. Short term ex-vivo expansion of circulating head and neck tumour cells. *Oncotarget* **2016**, *7*, 60101–60109. [CrossRef]
40. Koh, Y.; Yagi, S.; Akamatsu, H.; Kanai, K.; Hayata, A.; Tokudome, N.; Akamatsu, K.; Higuchi, M.; Kanbara, H.; Nakanishi, M.; et al. Heterogeneous Expression of Programmed Death Receptor-ligand 1 on Circulating Tumor Cells in Patients With Lung Cancer. *Clin. Lung Cancer* **2019**, *20*, 270–277.e271. [CrossRef]
41. Ilié, M.; Szafer-Glusman, E.; Hofman, V.; Chamorey, E.; Lalvée, S.; Selva, E.; Leroy, S.; Marquette, C.H.; Kowanetz, M.; Hedge, P.; et al. Detection of PD-L1 in circulating tumor cells and white blood cells from patients with advanced non-small-cell lung cancer. *Ann. Oncol.* **2018**, *29*, 193–199. [CrossRef]
42. Evrard, D.; Hourseau, M.; Couvelard, A.; Paradis, V.; Gauthier, H.; Raymond, E.; Halimi, C.; Barry, B.; Faivre, S. PD-L1 expression in the microenvironment and the response to checkpoint inhibitors in head and neck squamous cell carcinoma. *Oncoimmunology* **2020**, *9*, 1844403. [CrossRef]
43. Tu, X.; Qin, B.; Zhang, Y.; Zhang, C.; Kahila, M.; Nowsheen, S.; Yin, P.; Yuan, J.; Pei, H.; Li, H.; et al. PD-L1 (B7-H1) Competes with the RNA Exosome to Regulate the DNA Damage Response and Can Be Targeted to Sensitize to Radiation or Chemotherapy. *Mol. Cell* **2019**, *74*, 1215–1226.e1214. [CrossRef]
44. Satelli, A.; Batth, I.S.; Brownlee, Z.; Rojas, C.; Meng, Q.H.; Kopetz, S.; Li, S. Potential role of nuclear PD-L1 expression in cell-surface vimentin positive circulating tumor cells as a prognostic marker in cancer patients. *Sci. Rep.* **2016**, *6*, 28910. [CrossRef]

Printing copy of the publication 2

https://doi.org/10.1097/CCO.0000000000000935

Tinhofer I, Staudte S, George S. Liquid biopsy in head neck cancer: ready for clinical routine diagnostics? Curr Opin Oncol. 2023 May 1;35(3):151-157. doi: 10.1097/CCO.0000000000000935. Epub 2023 Mar 17. PMID: 36966499.

Curriculum Vitae

Mein Lebenslauf wird aus datenschutzrechtlichen Gründen in der elektronischen Version meiner Arbeit nicht veröffentlicht.

My CV will not be published in the electronic version of my work for data protection reasons.

Publication list

1. Tinhofer I, **Staudte S**, George S. Liquid biopsy in head neck cancer: ready for clinical routine diagnostics? Curr Opin Oncol. 2023 May 1;35(3):151-157. doi: 10.1097/CCO.0000000000000935. Epub 2023 Mar 17. PMID: 36966499.
2. **Staudte, S.**; Klinghammer, K.; Jurmeister, P.S.; Jank, P.; Blohmer, J.U.; Liebs, S.; Rhein, P.; Hauser, A.E.; Tinhofer, I. Multiparametric Phenotyping of Circulating Tumour Cells for Analysis of Therapeutic Targets, Oncogenic Signaling Pathways and DNA Repair Markers. Cancers (Basel) 2022, 14, doi:10.3390/cancers14112810.
3. Regan, J.L.; Schumacher, D.; **Staudte, S.**; Steffen, A.; Lesche, R.; Toedling, J.; Jourdan, T.; Haybaeck, J.; Golob-Schwarzl, N.; Mumberg, D.; Henderson, D.; Gyorffy, B.; Regenbrecht, C.R.A.; Keilholz, U.; Schafer, R.; et al. Identification of a neural development gene expression signature in colon cancer stem cells reveals a role for EGR2 in tumourigenesis. iScience 2022, 25, 104498, doi:10.1016/j.isci.2022.104498.
4. Regan, J.L.; Schumacher, D.; **Staudte, S.**; Steffen, A.; Lesche, R.; Toedling, J.; Jourdan, T.; Haybaeck, J.; Mumberg, D.; Henderson, D.; Gyorffy, B.; Regenbrecht, C.R.A.; Keilholz, U.; Schafer, R.; Lange, M. RNA sequencing of long-term label-retaining colon cancer stem cells identifies novel regulators of quiescence. iScience 2021, 24, 102618, doi:10.1016/j.isci.2021.102618.
5. Tinhofer, I.; **Staudte, S.** Circulating tumour cells as biomarkers in head and neck cancer: recent advances and future outlook. Expert Rev Mol Diagn 2018, 18, 897-906, doi:10.1080/14737159.2018.1522251.
6. Regan, J.L.; Schumacher, D.; **Staudte, S.**; Steffen, A.; Haybaeck, J.; Keilholz, U.; Schweiger, C.; Golob-Schwarzl, N.; Mumberg, D.; Henderson, D.; Lehrach, H.; Regenbrecht, C.R.A.; Schafer, R.; Lange, M. Non-Canonical Hedgehog Signaling Is a Positive Regulator of the WNT Pathway and Is Required for the Survival of Colon Cancer Stem Cells. Cell Rep 2017, 21, 2813-2828, doi:10.1016/j.celrep.2017.11.025.

Abstracts:

1. Regan, J.L.; **Staudte, S.**; Schumacher, D.; Keilholz, U.; Haybaeck, J.; Lehrach, H.; Yaspo, M.-L.; Henderson, D.; Steffen, A.; Toedling, J.; Lesche, R.; Schaefer, R.; Regenbrecht, C.R.A.; Mumberg, D.; Lange, M. Abstract 1715: Whole transcriptome analysis of patient-derived 3D in vitro and xenograft models of colon cancer identifies

placental genes required for the survival of cancer stem cells. Cancer Research 2016, 76, 1715-1715.

2. Regan, J.L.; **Staudte, S.**; Schumacher, D.; Keilholz, U.; Haybaeck, J.; Lehrach, H.; Yaspo, M.-L.; Henderson, D.; Steffen, A.; Toedling, J.; Lesche, R.; Schaefer, R.; Regenbrecht, C.R.A.; Mumberg, D.; Lange, M. Abstract 1714: The role of Hedgehog signaling in the regulation of human colon cancer stem cells. Cancer Research 2016, 76, 1714-1714.
3. Regan, J.L.; Schumacher, D.; **Staudte, S.**; Boehnke, K.; Keilholz, U.; Haybaeck, J.; Lehrach, H.; Henderson, D.; Schaefer, R.; Regenbrecht, C.R.A.; Mumberg, D.; Lange, M. Abstract 977: 3D-models of patient-derived colon tumours for the identification of genetic factors important in the regulation of cancer stem cells. Cancer Research 2015, 75, 977-977.

Acknowledgments

An dieser Stelle möchte ich mich bei meiner Doktormutter Frau Prof. Dr. Ingeborg Tinhofer-Keilholz dafür bedanken, dass Sie es mir mit Ihrem Ehrgeiz und Engagement ermöglicht hat, in Ihrem Labor meine Doktorarbeit anzufertigen. In der Zeit meiner Promotion hatten wir sehr viele interessante und inspirierende wissenschaftliche Diskussionen zu meinen Daten und den daraus resultierenden Hypothesen, an denen ich als Wissenschaftlerin wachsen konnte und viel für mich gelernt habe. Auch möchte ich Ihr für ihr Vertrauen in mich und meine Expertise danken und die damit einhergehende Unterstützung und stetige Förderung.

Ich möchte hier auch Prof. Dr. Ulrich Keilholz danken, für die regen und aufschlussreichen Diskussionen zu den klinischen Aspekten meiner Dissertation. Ebenso danke ich PD Dr. Konrad Klinghammer für seine intensive Unterstützung in der Entwicklung meiner Studienfragestellung als auch für die anschließende Patientenrekrutierung. Herr PD Dr. Klinghammer stand mir ebenfalls mit Rat und Tat zur Seite, wenn ich Fragen zum medizinischen Verständnis hatte und auch bei der Aufbereitung der klinischen Daten für die von mir anschließend durchgeführte statistische Auswertung.

Ein besonderer Dank geht an dieser Stelle an die Patient*innen und ihren Familien, welche mir durch ihre Einwilligung zur Studienteilnahme die Erstellung dieser Arbeit erst ermöglicht haben.

Zu guter Letzt gilt mein größter Dank meiner Familie und meinen Freunden, die mich durch all die Höhen und Tiefen begleitet haben, die mich während meiner Dissertation herausgefordert haben. Sie haben meine Erfolge mit mir gefeiert, die großen wie die kleinen, meine Begeisterung an meinem Projekt mit Freude wahrgenommen, mich auch bei Rückschlägen begleitet und motiviert weiterzugehen. Insbesondere möchte ich an dieser Stelle meinem Vater Andreas Staudte für die vielen fachlichen und philosophischen Diskussionen danken, aber ebenso für die immerwährende emotionale Unterstützung. Sein Vertrauen in mich und mein Können, welches mir auch von seiner Frau Anett Staudte-Werner und meinen Großeltern Elke und Gerhard Kölpin stets entgegengebracht wurde, haben mich immer wieder dazu ermutigt diesen Weg weiterzugehen. Sandra Liebs möchte ich an dieser Stelle für die wundervolle Freundschaft danken, die sich aus einem Kolleginnenverhältnis entwickelt hat. Dafür bin ich sehr dankbar. Aber auch für ihren unermüdlichen Input, wenn Fragen zu

Experimenten aufgekommen sind oder ich Bedarf nach einer anderen Sichtweise auf meine Daten hatte, stand sie mir jederzeit mir Rat und Tat zur Seite.

Auf den letzten Metern zur Fertigstellung meiner Dissertation konnte ich auf die Motivationskraft meines Partners Christian Frank setzen, welcher nie müde wurde, mich zu motivieren, meinen Fokus immer wieder auf die Niederschrift meiner Promotion zu setzen.

Abschließend möchte ich an dieser Stelle noch erwähnen, dass ich jedem einzelnen der mich auf diesem Weg begleitet und unterstützt hat vom Herzen danke.